Available online at www.sciencedirect.com

ScienceDirect

Geochimica et Cosmochimica Acta 303 (2021) 223–248

Geochimica et Cosmochimica Acta

www.elsevier.com/locate/gca

The role of magmatism in hydrocarbon generation in sedimented rifts: A Nd isotope perspective from mid-Cretaceous methane-seep deposits of the Basque-Cantabrian Basin, Spain

M. Jakubowicz [a,*], L.M. Agirrezabala [b], J. Dopieralska [c], M. Siepak [d], A. Kaim [e], Z. Belka [a]

[a] *Isotope Research Unit, Adam Mickiewicz University, ul. B. Krygowskiego 10, 61-680 Poznań, Poland*
[b] *Department of Geology, University of the Basque Country UPV/EHU, Sarriena auzoa z/g, 48940 Leioa, The Basque Country, Spain*
[c] *Poznan Science and Technology Park, Adam Mickiewicz University Foundation, ul. Rubież 46, 61-612 Poznań, Poland*
[d] *Institute of Geology, Adam Mickiewicz University, ul. B. Krygowskiego 12, 61-680 Poznań, Poland*
[e] *Institute of Paleobiology, Polish Academy of Sciences, ul. Twarda 51/55, 00-818 Warszawa, Poland*

Received 31 May 2020; accepted in revised form 24 March 2021; Available online 2 April 2021

Abstract

Studies on the involvement of intrusive magmatism in hydrocarbon generation within sedimentary basins have gained momentum owing to increasing appraisal of the role that such processes may play in controlling global carbon cycle perturbations, and the exploration potential of the volcanic sedimentary basins. Nevertheless, for many areas the causal link between the intrusions and surrounding hydrocarbon systems remains disputed, encouraging a search for methods that could aid in identifying different hydrocarbon sources. Here, we have performed a multi-proxy geochemical study of the middle Cretaceous methane-seep deposits of the Basque-Cantabrian Basin, an early-stage, peri-cratonic rift marking the Mesozoic opening of the Bay of Biscay. Infilled by a thick sedimentary succession intruded by shallow-level igneous bodies, the basin shares analogies with modern young, sedimented rifts that sustain hydrocarbon seepage. We have applied a novel approach that uses the Nd isotope composition of the seep deposits to constrain the relationship between hydrocarbon seepage and igneous activity, and to explore the general potential of Nd isotopes to trace magmatic-influenced fluids in volcanic sedimentary basins. The Nd isotope data have been combined with rare earth element analyses and carbon and oxygen isotope measurements, providing broad insight into the former composition of the seeping fluids. For three out of four investigated seeps, the Nd isotope ratios observed in authigenic seep carbonates include signatures markedly more radiogenic than that reconstructed for background seawater-derived pore waters. The level of this ^{143}Nd-enrichment varies both between and within individual deposits, reflecting spatial and temporal differences in fluid composition typical of seep-related environments. The radiogenic Nd isotope signals provide evidence of subseafloor interactions between the seeping fluids and mafic igneous materials, supporting the model of an igneous control on the mid-Cretaceous methane expulsion in the Basque-Cantabrian Basin. The thermogenic origin of the methane is in accord with the moderately negative δ^{13}C values and paragenetic successions observed in the studied seep carbonates. For a single deposit, its relatively unradiogenic Nd isotope composition can be attributed to the smallest size and shallowest emplacement depth of the underlying intrusion, likely resulting in a short-lived character and limited hydrocarbon-generation potential of the associated contact metamorphism. The study demonstrates that Nd isotope analyses of seep carbonates offer a tool in disentangling methane fluxes from different organic matter alteration pathways

* Corresponding author.
E-mail address: mjakub@amu.edu.pl (M. Jakubowicz).

https://doi.org/10.1016/j.gca.2021.03.025

for the numerous, both fossil and modern sedimented rifts for which the involvement of various methane sources remains insufficiently understood.

Keywords: Cold seeps; Seep and vent carbonates; Volcanic sedimentary basins; Sedimented rifts; Thermogenic hydrocarbons; Hydrothermal systems; Albian; Neodymium isotopes; Carbon and oxygen isotopes; Rare earth elements

1. INTRODUCTION

Sedimentary basins affected by intrusive magmatism, including, most notably, continental rifts and buried sections of mid-ocean ridges, host some of the most complex fluid expulsion systems known from Earth's oceans (Einsele et al., 1980; Simoneit, 1994; Cruse and Seewald, 2006; Teske et al., 2019). Filled with thick, commonly organic-rich sedimentary packages affected by magmatic heat transfer, the sedimented rifts represent rare settings that can sustain both high-temperature hydrothermal vents and more temperate, hydrocarbon-dominated, cold seeps (Simoneit et al., 1988; Paull et al., 2007; Lizarralde et al., 2011; Núñez-Useche et al., 2018). Both these end-member types of fluid emissions may be juxtaposed against each other across small distances, and some areas sustain seepage of fluids combining components of multiple sources (Welhan and Luton, 1987; Seewald et al., 1994; Geilert et al., 2018; Snyder et al., 2020). Studies of such transitional, magmatic-sedimentary systems hold the key to advance our understanding of the role of magmatism in hydrocarbon expulsion from sedimentary basins, a question that has received increasing attention (Schutter, 2003; Lizarralde et al., 2011; Svensen et al., 2015; Schofield et al., 2017). Recently, a number of studies highlighted the importance of igneous processes not only in hydrogeological evolution of buried rifts, but also their large-scale impact on the global carbon cycle and climate perturbations (Svensen et al., 2004, 2007; Aarnes et al., 2015; Berndt et al., 2016).

So far, comprehensive reconstructions of hydrocarbon generation patterns in either modern or fossil sedimented spreading centres have been relatively rare. From a geological standpoint, the most significant of the difficulties involved in such studies is the typically limited knowledge of basement configurations of individual seep and vent systems. Given the deep-marine setting and complex tectonic architecture of rifted margins, the extent and composition of rift-filling sediment blankets, distribution and geometry of igneous intrusions, and fluid-channelling horizons must be interpreted primarily based on geophysical data (Fisher and Narasimhan, 1991; Svensen et al., 2004; Lizarralde et al., 2011; Geilert et al., 2018; Sydnes et al., 2018). Chief among these are seismic images, interpretation of which remains inherently difficult (Schofield et al., 2017), and commonly inconclusive with respect to fluid flow patterns (cf., Cartwright and Santamarina, 2015; Angkasa et al., 2017). This is accompanied by a limited number of modern rifts for which hydrocarbon seepage has been documented in sufficient detail to allow for a broader appraisal of fluid circulation. Among modern rifts known to sustain extensive hydrocarbon seeps, only for the Guaymas Basin, Gulf of California, have the seismic, petrological and geochemical investigations been advanced enough to allow deeper discussions on fluid sources (Welhan and Lupton, 1987; Simoneit, 1994; Paull et al., 2007; Berndt et al., 2016).

Geological characteristics of continental rift-hosted fluid discharges can be better understood by examination of fossil sedimentary basins influenced by volcanic activity, some of which offer extensive exposures of plumbing systems that fed ancient seeps and vents (e.g., Gaillard et al., 1992; Jamtveit et al., 2004; Svensen et al., 2007; Angkasa et al., 2017). In such cases, studies of fluid origin must rely on petrological and geochemical systematics of authigenic minerals. Most characteristic of these are methane-seep carbonates, which precipitate from shallow-burial pore waters as by-products of increase in pore water alkalinity driven by anaerobic oxidation of methane by chemoautotrophic microbes (Knittel and Boetius, 2009). For buried rifts, of particular utility in such investigations are geochemical techniques able to detect former fluid-rock interactions involving mafic igneous rocks, such as rare earth element (REE) patterns, as well as Sr and Nd isotope analyses (e.g., Piepgras and Wasserburg, 1985; Craddock et al., 2010; Geilert et al., 2018; Jakubowicz et al., 2019). The latter, traditionally applied for fluid tracing at unsedimented hydrothermal vents, have recently been shown to provide a sensitive tool of recognising the former presence of volcanic-derived fluid components in sedimentary systems (Jakubowicz et al., 2015, 2019). When combined with structural data and diagenetic histories of given seep occurrences, these radiogenic isotope and trace element methods enable insights notably beyond those provided by traditionally used C and O isotope measurements (Jakubowicz et al., 2015, 2020; Ge et al., 2020).

In the present contribution, we have performed a multiproxy geochemical study of four mid-Cretaceous hydrocarbon-seep deposits of the Basque-Cantabrian Basin (northern Spain). Having developed within an incipient continental rift, these carbonates represent some of the best exposed fossil seeps associated with a volcanic-affected sedimentary basin (Agirrezabala, 2009, 2015; Agirrezabala et al., 2013; Wiese et al., 2015). They afford, therefore, a rare opportunity for a detailed reconstruction of the relationships between the seep deposits and different elements of their former plumbing systems. Based on the combination of tectonic constraints, indirect evidence from petrological and geochemical data, and the presence of igneous bodies underlying the seep deposits, it has been hypothesised that hydrocarbons originated in the Basque-Cantabrian Basin as a result of thermal alteration of the rift-filling sediments by subvolcanic intrusions (Agirrezabala, 2009, 2015; Agirrezabala and Dinarès-Turell, 2013; Agirrezabala et al.,

2013). Here, we test this scenario by combining Nd, stable isotope and REE analyses of the methane-derived carbonates. Our results provide new data on the fluid generation history of the Basque-Cantabrian Basin, and, on a more general scale, allow for exploring the general applicability of the Nd isotope system to identify fluid sources in sedimented rift-hosted hydrocarbon systems.

2. GEOLOGICAL SETTING

2.1. General context

The studied seep deposits are exposed along the coast of the Basque Country, in the northern part of the Mesozoic Basque-Cantabrian Basin (Fig. 1A). The basin represents the westernmost part of the Pyrenean-Cantabrian mountain belt, as a whole marking the Iberia-Eurasia plate boundary (DeFelipe et al., 2018). The Mesozoic sedimentary basins rimming the northern margin of Iberia record a complex series of tectonic events and plate motions that preceded the orogeny. Starting from the late Palaeozoic and through much of the Mesozoic, the Pyrenean domain was subjected to extensional to transtensional tectonics, whose structural and stratigraphic expressions varied spatially as a result of its strong structural segmentation (Jammes et al., 2009; Tugend et al., 2015; Teixell et al., 2018). The Basque-Cantabrian Basin originated as a relatively narrow, oblique peri-cratonic rift associated with

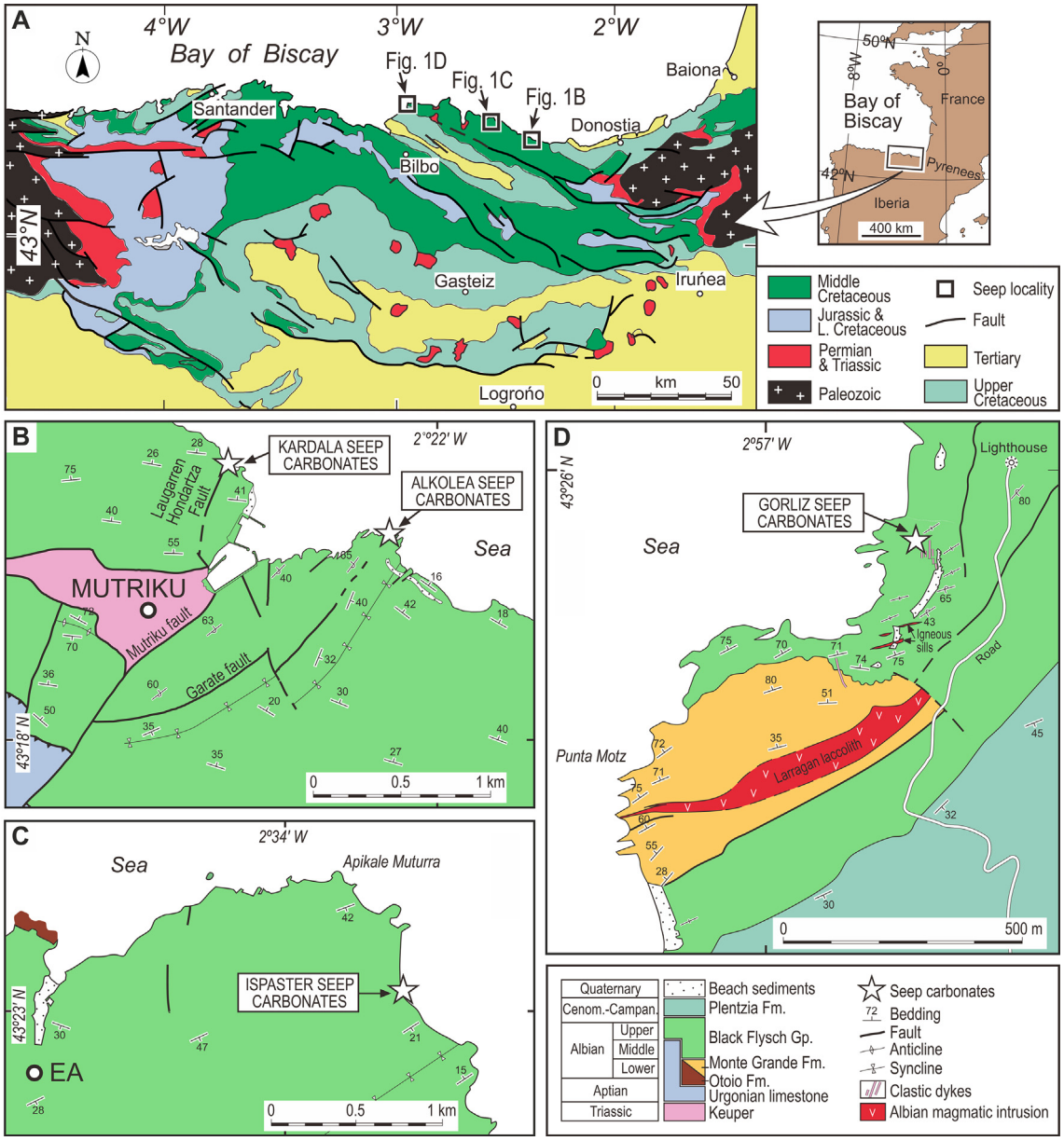

Fig. 1. Generalised geological maps of the Basque-Cantabrian Basin (**A**) and studied localities (**B**: Kardala and Alkolea; **C**: Ispaster; **D**: Gorliz), with indicated occurrences of the Albian seep deposits.

the opening of the Bay of Biscay and North Atlantic Ocean. During the main, Aptian to Cenomanian phase of its development, the basin represented one of the most intensely subsiding areas of the Pyrenean realm, and the main depocentre in its western part (Rat, 1988; García-Mondéjar et al., 1996). The basin formation followed the development of a regional transtensional regime, accompanying the onset of seafloor spreading in the Bay of Biscay, and associated left-lateral drift of Iberia. These processes culminated in the Albian, for which a range of tectonic features indicative of strike-slip tectonics have been documented (García-Mondéjar et al., 1996; Agirrezabala and Dinarès-Turell, 2013).

By the middle Cretaceous, the continuous lithospheric extension along most of the Iberia-Eurasia boundary resulted in development of a complex system of hyperextended rifts connecting the Atlantic and Tethys oceans, in places marked by zones of mantle unroofing (Pedrera et al., 2017; DeFelipe et al., 2018; Teixell et al., 2018). For the Basque-Cantabrian area, the crustal hyperthinning was particularly pronounced in its eastern part, for which mantle unroofing occurred to the base of the basin-filling sedimentary succession during the late Albian, with exhumation of a narrow peridotite domain (DeFelipe et al., 2017). Across the basin, this was accompanied by mafic volcanism and emplacement of subvolcanic intrusions, starting from the late Barremian, and culminating during late Albian – Santonian time (Castañares et al., 2001; Ubide et al., 2014; García-Mondéjar et al., 2018). The volcanic activity was focused in the central and northern parts of the basin, for which a number of outcrops have been studied (Rossy et al., 1992; Ubide; Agirrezabala et al., 2014, 2017; Garcia-Mondejar et al., 2018). Except for these, several intrusions have been identified in seismic images (Agirrezabala and Dinarès-Turell, 2013; Agirrezabala et al., 2013). Among the outcrops, the continental tectonic setting and both effusive and intrusive origin of the volcanics are reflected in their petrographic variability. Dominant are basaltoids (basalts, teschenites, basaltic trachyandesites), sometimes with ultramafic cumulates (picrites), with a subordinate role of gabbros and syenites (Rossy et al., 1992; Ubide). The magma ascent was facilitated by a system of deep, NW-SE trending faults, which compartmentalised the basin and played part in local high-temperature metamorphism and hydrothermal mineralisation (Velasco et al., 2003; López-Horgue et al. 2010). Geochemically, the volcanics display signatures distinct from those of mid-ocean ridge basalts and similar to the mantle source of oceanic island (HIMU- and EM-1-type) basalts, recording contribution of continental material and resembling volcanics known from other infant rifts (Rossy et al., 1992; Ubide). These geochemical systematics are consistent with structural observations, implying that, despite the extreme crustal thinning, the Basque-Cantabrian rift failed to reach the seafloor-spreading stage. The extensional period of its evolution lasted until the Cenomanian. By the late Santonian, the plate configuration around Iberia evolved towards a compressional regime, which resulted in basin inversion during the Paleogene (Teixell et al., 2018).

2.2. Seep deposits

All studied seep deposits are hosted by primarily argillaceous turbidite successions of mudstones, sandstones and conglomerates that infill the numerous subbasins of the northern-central part of the Basque-Cantabrian Basin, jointly referred to as the Black Flysch Group (Middle Albian – Lower Cenomanian; Souquet et al., 1985; Figs. 1 and 2A,H). This thick, organic-rich unit was deposited in a relatively deep-water, bathyal setting (200–2000 m as implied by foraminifera data; Rodriguez Lazaro et al., 1998; Castañares et al., 2001; García-Mondéjar et al., 2004). The Black Flysch Group crops out across the Pyrenean domain and is divided into numerous local, mostly informal lithostratigraphic units (see Agirrezabala, 2009, 2015; Agirrezabala et al., 2013 and references therein). Because of spatial differences in tectonic regimes and subsidence rates in different portions of the Basque-Cantabrian area, the Black Flysch siliciclastics, deposited in structural troughs, grade laterally into shallower-water, carbonate-dominated deposits representative of structural highs, with local development of rudist-rich carbonate platforms (Aptian – Albian 'Urgonian Complex'; García-Mondéjar, 1990).

The seep deposits are scattered within the Black Flysch Group in the form of irregular carbonate bodies, concentrated at four sites (Figs. 2 and 3), all of which have been studied in the present contribution. Stratigraphically, all these seeps fall within a narrow interval of two upper Albian ammonite subzones (*Hysteroceras varicosum* – *Callihoptiles auritus*), approximately corresponding to the main phase of magmatism in the northern Basque-Cantabrian Basin (*auritus* Subzone, Castañares et al., 2001; ~102 Ma as dated by $^{40}Ar/^{39}Ar$ ages, Ubide et al., 2014). For each of these deposits, their seep-related origin has been documented based on their geological backgrounds, paragenetic sequences, biota and, in particular, strongly negative $\delta^{13}C_{carbonate}$ values, recording incorporation of ^{13}C-depleted carbon indicative of microbial oxidation of methane (Agirrezabala, 2009, 2015; Agirrezabala et al., 2013; Wiese et al., 2015).

2.2.1. Kardala and Alkolea sites

Two accumulations of seep carbonates, referred to as the Kardala and Alkolea seeps, ~1 km apart, are found near the village of Mutriku in the north-eastern part of the Basque-Cantabrian Basin (Fig. 1B; Agirrezabala et al., 2008; Agirrezabala, 2009). The deposits formed within the *auritus* Subzone on opposite sides of a major structural boundary comprised by the deep, high-angle Mutriku fault (Figs. 1B and 4A). Both the fault development and its apparent role in channeling the methane seepage were associated with vertical-axis rotation of the Deba block to the south-east (Agirrezabala and Dinarès-Turell, 2013). Except the seep limestones, sediments adjacent to the fault host upper Albian hydrothermal mineralisations and metalliferous deposits (EEE, 2003).

The Kardala seep developed along the Laugarren Hondartza fault, a minor discontinuity branching off from the Mutriku fault (Fig. 1B). The seep carbonate-hosting Black

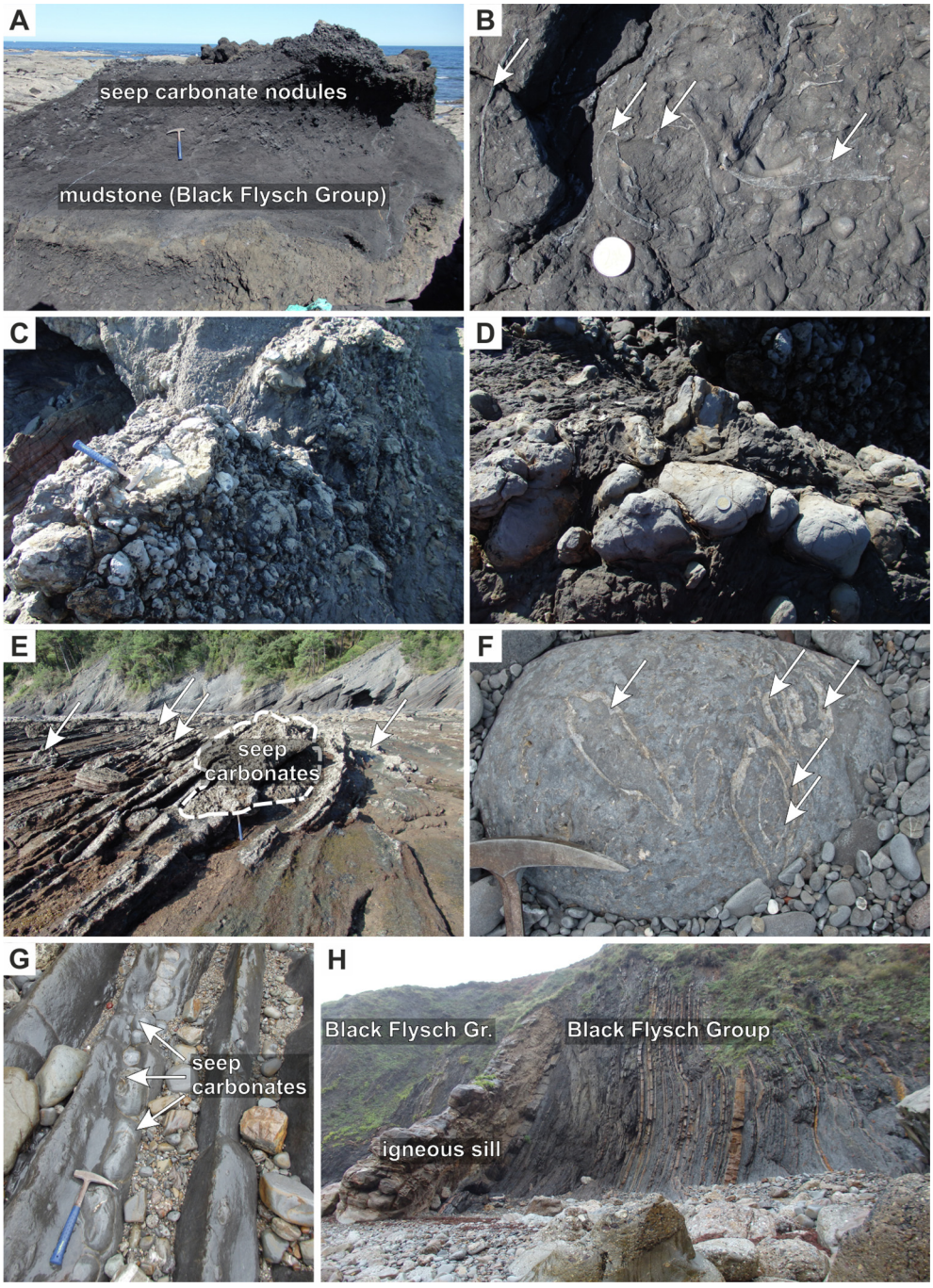

Fig. 2. Occurrence modes and geological context of the Albian seep carbonates of the Basque-Cantabrian Basin. **A – B**. Numerous, relatively small carbonate nodules making up the Kardala deposit. Note the presence of bivalves of the family Lucinidae (arrows in B), a group with a long evolutionary history in seep-related ecosystems. Hammer (A) and coin (B) for scale. **C – D.** Accumulation of numerous, irregular carbonate lenses comprising the Alkolea deposit. Hammer (C) and coin (D) for scale. **E – F.** Carbonate bodies of the Ispaster deposit. A large, *in situ* seep-carbonate lens is indicated with a dashed-line border; several smaller lenses are indicated with arrows in E. Note the presence of large, *Caspiconcha* bivalves, typical of Mesozoic seep-related communities (arrows in F). Hammer for scale. **G – H.** Small seep-carbonate bodies (G) and one of the igneous sills (H; sill A in Fig. 4) exposed in the Gorliz section. The sill is enveloped by a contact metamorphic aureole developed by thermal alteration of argillaceous sediments of the Black Flysch Group (Agirrezabala et al., 2014). Hammer (G) for scale; the sill (H) is max. 5 m-thick.

Flysch Group is exposed here as a continuous, 500–1000 m-thick succession dominated by sandy mudstones with rare sandy turbidites. The seep limestones occur in the form of a ~ 5 m-thick and 16 m-long, lensoidal accumulation of nodules, concretionary beds and tubular concretions (Fig. 2A,B). The structural position and geometry of the

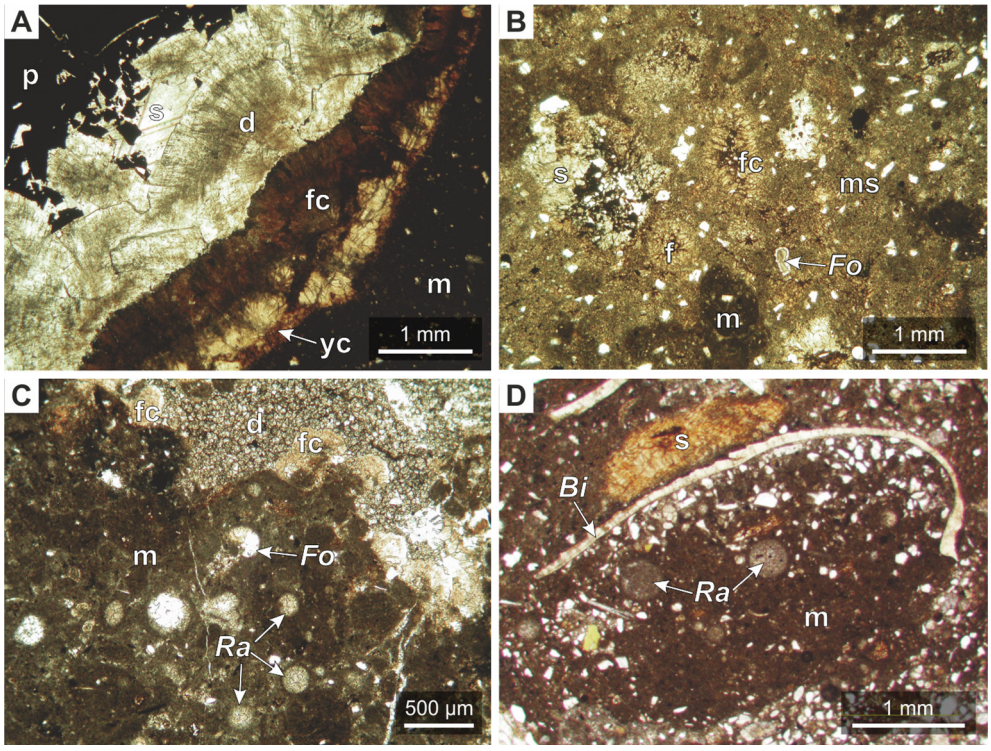

Fig. 3. Representative photomicrographs of the Albian seep carbonates of the Basque Cantabrian Basin: the Kardala (**A**), Alkolea (**B**), Ispaster (**C**) and Gorliz (**D**) deposits. For all sites, volumetrically dominant is pyrite-rich, micritic to microsparitic calcite, hosting abundant mud- to sand-sized siliciclastic particles (A – D), foraminifera and radiolarian microfossils (B – D) and bivalves (D). The micrite shows frequent dissolution cavities (A – D) filled by early-diagenetic yellow calcite and botryoidal fibrous calcite (A – C), and later-diagenetic dolomite, sparry calcite and pyrobitumen (A – D). Abbreviations: m – micrite; ms – microspar; s – spar; yc – yellow calcite; fc – fibrous calcite; d – dolomite; p – pyrobitumen; *Fo* – foraminifera; *Ra* – radiolarian; *Bi* – bivalve.

seep deposit suggest fluid migration through the Laugarren Hondartza-Mutriku fault system (Agirrezabala, 2009; Fig. 4A). As is typical of seep precipitates, the Kardala carbonates display high variability in cement fabrics, recording periods of carbonate authigenesis intermingled with dissolution events (Fig. 3A). Volumetrically dominant is calcitic, pyrite-rich micrite, precipitated as the earliest cement generation in sediment pore spaces. This phase engulfs abundant macrofossils, most notably members of the seep-dwelling, chemosymbiotic bivalve family Lucinidae (Fig. 2B). The seep-related origin of the micrite is attested by its low $\delta^{13}C$ values, reaching down to −17.3‰ (Agirrezabala, 2009; for compilation of previously published stable isotope data, see Fig. 5 and Supplementary Table 1). Dissolution cavities truncating the micrite have been infilled by sparry cements, dominated by early-diagenetic, irregular sparry mosaic ('yellow calcite') and isopachous fibrous calcite, the latter displaying a botryoidal fabric and most pronounced ^{13}C-depletion (Agirrezabala, 2009). Among later-diagenetic cements, most conspicuous are saddle dolomite with solid bitumen inclusions, widespread solid bitumen (impsonite) occluding intercrystalline spaces, and blocky calcite spar infilling final void spaces.

The general geological context of the Alkolea deposit is more complex than that of the Kardala carbonates (Fig. 4A; see Fig. 2 in Agirrezabala and Dinarès-Turell, 2013). The Black Flysch Group is here composed of mudstones with relatively frequent sandy intercalations. The Alkolea deposit both overlies and is overlain by angular unconformities, associated with two stages of development of the Aitzeta syncline, the main structural feature to the south-east of the Mutriku Fault (Agirrezabala et al., 2002; Agirrezabala and Dinarès-Turell, 2013). The seep carbonates occur within a lenticular, ~8 m-thick and 40 m-long accumulation as nodules, lenses, septarias and carbonate breccias (Fig. 2C,D). The sole seep-related macrofossils are rare, *Hikidea*-like gastropods. A dominant early-diagenetic phase is micrite (Fig. 3B), showing pronounced ^{13}C-depletion ($\delta^{13}C = -8.6$ to −24.4‰; Agirrezabala, 2009; Fig. 5). The former open spaces are mostly rimmed by isopachous fibrous cement, with $\delta^{13}C$ values as low as −41.5‰ (Agirrezabala, 2009). The later-diagenetic stage is dominated by blocky spar, with rare pyrobitumen fills. In addition, centres of some concretions have been occluded with a hydrothermal association of sulphate minerals (celestine, barite, gypsum and anhydrite), carbonates and albite (Agirrezabala, 2009).

A seismic reflection profile available for the south-western part of the Deba block, close to the occurrence of the Kardala and Alkolea deposits, documents the presence of two highly reflective bodies at a depth of ~0.7 s (Fig. 12 in Agirrezabala and Dinarès-Turell, 2013). Assuming a conservative mean seismic velocity of 4500 m/s, documented for shallow sedimentary rocks from a nearby commercial

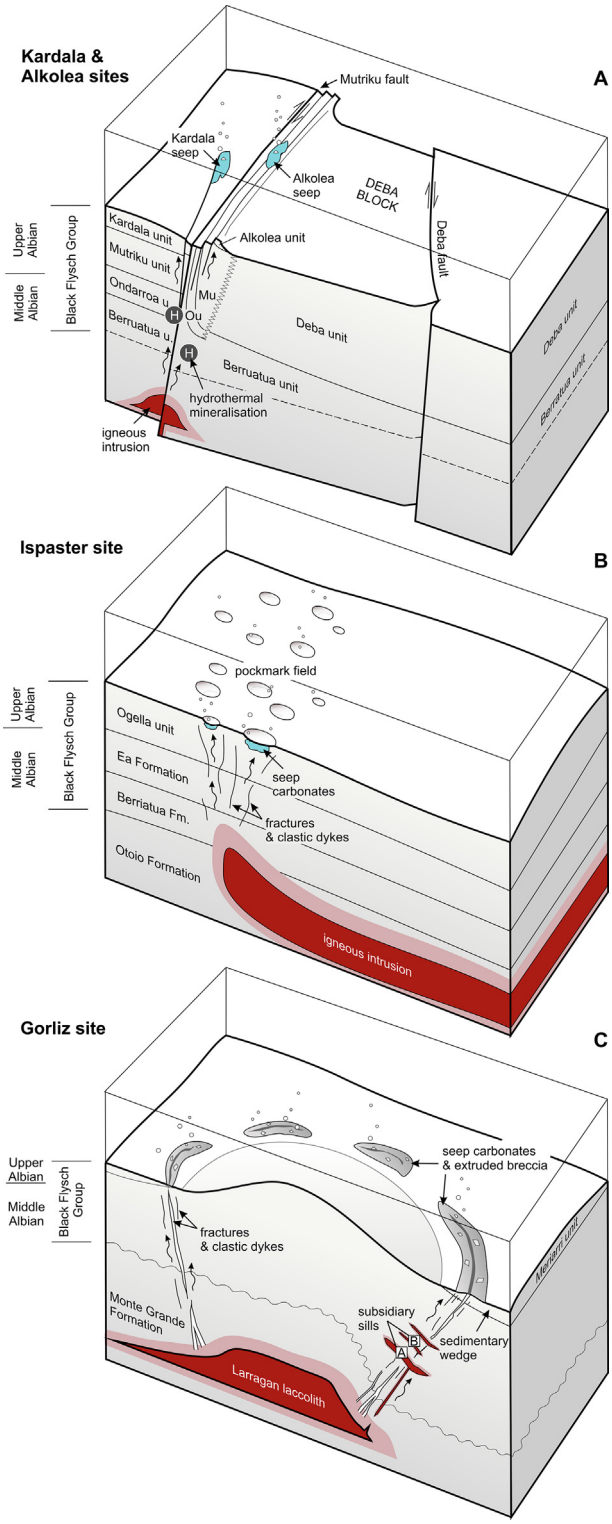

Fig. 4. Schematic illustration of the relationships among the Albian seep deposits of the Basque-Cantabrian Basin, their basement configurations and plumbing systems, and the role of igneous intrusions, based on models developed by Agirrezabala and Dinarès-Turell (2013; **A**: Kardala and Alkolea deposits), Agirrezabala et al. (2013; **B**: Ispaster deposit) and Agirrezabala (2015; **C**: Gorliz deposit). Chrono- and lithostratigraphies of individual sections, including both formal and informal units, are shown as well (see Agirrezabala, 2009, 2015; Agirrezabala and Dinarès-Turell, 2013; Agirrezabala et al., 2013 for details).

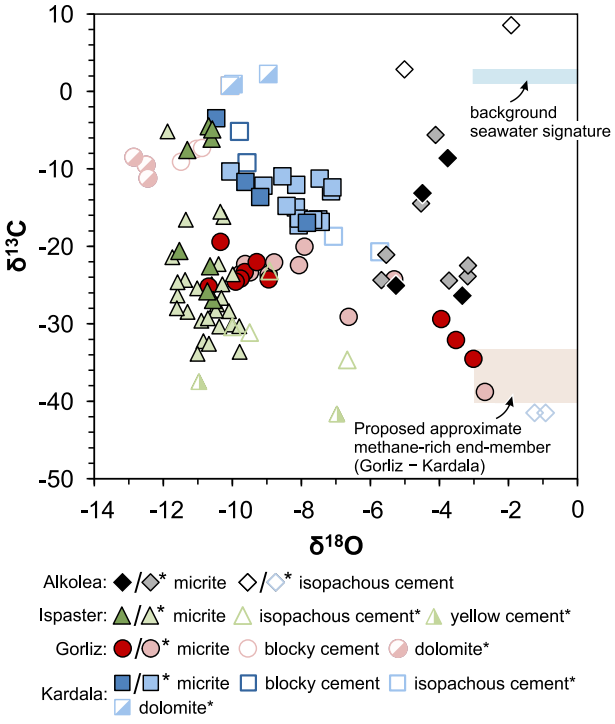

Fig. 5. C vs. O isotope cross-plot for the Albian seep deposits of the Basque-Cantabrian Basin. Data from previous studies are plotted for comparison (asterisks; Kardala, Alkolea: Agirrezabala, 2009; Ispaster: Agirrezabala et al., 2013; Gorliz: Agirrezabala, 2015; see Supplementary Table 1).

well (Gaviota field; Huedo-Cuesta et al., 2009), this corresponds to the present depth of ~800 m, and, when corrected for compaction, inferred original emplacement depth of ~1500 m (Table 1). Both bodies show dimensions, geometries and seismic expression typical of magmatic laccoliths, with concordant, high-amplitude reflections, convex-up tops and flat bases, thus being interpreted as igneous intrusions (Agirrezabala and Dinarès-Turell, 2013; Fig. 4A). This interpretation is corroborated by the Albian hydrothermal mineralisations found in the area, exposures of Albian igneous intrusions ~4 km to the south-west (EEE, 2003), and general abundance in the northern Basque-Cantabrian Basin of volcanic and subvolcanic rocks penecontemporaneous with the seep deposits (Castañares et al., 2001; Ubide et al., 2014). The igneous character of the high-amplitude structures is also in agreement with their position in the part of the Deba block subjected to late Albian extension, as such areas are typically favoured as loci of magma ascent in strike-slip settings (cf., Tibaldi et al., 2010; Agirrezabala and Dinarès-Turell, 2013).

2.2.2. Ispaster site

Fifteen km to the north-west of the two sites associated with the Mutriku Fault, another accumulation of seep carbonates is exposed to the north of the village of Ispaster (Fig. 1C; Agirrezabala et al., 2013; Kiel, 2013, Wiese et al., 2015; Jenkins et al., 2018). The Black Flysch Group reaches a local thickness of ~800 m and is dominated by mudstones with common sandy turbidites. The Ispaster carbonates form two horizons, dated to *varicosum – auritus* subzones and spatially associated with several, contemporaneous sandstone dykes. Agirrezabala et al. (2013) interpreted the deposit geometry, together with its relationship to local sandstone lenses, as indicative of a pockmark-related origin of the Ispaster seep (Fig. 4B).

The seep carbonates occur mostly as concretions and lenses (Fig. 2E,F), some > 8 m across, made up primarily of calcitic, pyrite- and peloid-rich micrite (Fig. 3C). The micrite hosts common macrofossils, including clusters of the large kalenterid bivalve *Caspiconcha basquensis* Jenkins et al., 2018 (Fig. 2F), and scarcer lucinid bivalves (*Tehamatea agirrezabalai* Kiel, 2013), as well as worm tubes and *Hokkaidoconcha* gastropods, all typical of Cretaceous seep communities. The micritic matrix displays marked ^{13}C-depletion ($\delta^{13}C_{min} = -33.8‰$; Agirrezabala et al., 2013; Fig. 5). Early-diagenetic cements infilling small empty spaces are typically developed as isopachous, yellow and/or fibrous calcite, reaching $\delta^{13}C$ values of down to −41‰ (Agirrezabala et al., 2013). Central parts of some voids have been occluded with blocky calcite and, locally, dolomite, solid bitumen and/or barite crystals.

A seismic profile collected for the study area (Fig. 21 in Agirrezabala et al., 2013) images at least two high-amplitude structures at depths of 0.5 s and 0.75 s, translat-

Table 1
Compilation of the emplacement-depth and geometry data for the subvolcanic intrusions underlying the Albian seep deposits of the Basque-Cantabrian Basin.

Intrusion	Original depth (compacted)	Original depth (uncompacted)[□]	Geometry (width × thickness)
Mutriku[*]	790 m[†]	1530 m	Two laccoliths, each ~1000 × 60(?) m[§]
Ispaster[#]	800 m and 1190 m[†]	1490 m and 2160 m	Two sills, each ~3000 × 60(?) m[§]
Gorliz[±]	265 m	450 m	Laccolith 600 × 40 m, with subsidiary sills

[*] Intrusion underlying the Kardala and Alkolea seep deposits; imaged seismically (Agirrezabala and Dinarès-Turell, 2013).
[#] Imaged seismically (Agirrezabala et al., 2013).
[±] Larragan laccolith system (Agirrezabala et al., 2014; Agirrezabala, 2015).
[†] Decompation method after Einsele (2000).
[□] Corrected for local dips (Ispaster: ~20°; Gorliz: ~60°); assumed seismic velocity of 4500 m/s (see text).
[§] Approximate geometries based on seismic data.

ing into uncompacted depths of ~1500 and ~2200 m (Table 1). As for the Kardala-Alkolea area, the combination of the high reflectivity of these structures, their relationship with the surrounding strata and general geometries have been interpreted as indicative of their intrusive igneous origin (Agirrezabala et al., 2013; Fig. 4B). This interpretation is supported by the position of the Ispaster seep approximately at the periphery of the inferred igneous body, which corresponds to the typical position of fluid expulsion systems accompanying subvolcanic intrusions (cf., Planke et al., 2005; Schofield et al., 2010; Iyer et al., 2013). Furthermore, an intrusive episode is in consonance with the presence of the pockmarks and clastic dykes, representing surface expressions of rapid discharge of overpressured fluids (cf., Cartwright and Santamarina, 2015). Likewise, according to Agirrezabala et al. (2013), the clastic dykes correspond to peripheral fractures formed along the intrusion margin, providing pathways for the former methane advection (Fig. 4B). Indeed, the stratigraphic depth of the proposed intrusions places the deeper structure within the Otoio Formation, which underlies the Black Flysch Group (Fig. 4B), in agreement with abundant rock fragments of this unit found in the dykes (Agirrezabala et al., 2013).

2.2.3. Gorliz site

The westernmost seep deposit of the Basque-Cantabrian Basin is located near the village of Gorliz, 33 km to the north-west of the Ispaster site (Fig. 1D; Agirrezabala, 2015). The Black Flysch Group is exposed here as a > 200 m-thick package of mudstones with subordinate sandstones and conglomerates. The seep carbonate-hosting part of this succession, dated to the *varicosum* Subzone, is dominated by sandstones, which form a well-defined sedimentary wedge overlying a local forced fold (Agirrezabala, 2015).

The seep carbonates are scattered within the sedimentary wedge as irregular lenses, nodules, concretions and septarias, typically concentrated along bedding planes (Fig. 2G). Compared to the other Basque seeps, the carbonate bodies are here noticeably scarcer and typically small (max. 40 cm across). The dominant texture is calcitic, pyrite-enriched micrite (Fig. 3D), showing strongly negative $\delta^{13}C$ values (down to 38.7‰; Agirrezabala, 2015; Fig. 5). The micrite hosts rare fossils of unidentified bivalves and gastropods. The former open spaces have been occluded by early fibrous calcite, blocky calcite and, ultimately, saddle dolomite crystals.

The late Albian fluid expulsion at Gorliz has additionally been recorded in the form of clastic dykes cross-cutting the sedimentary wedge. Compared to the Ispaster site, the Gorliz dykes are notably more common and contain particularly frequent, large (up to 0.5 m across) clasts composed of siliciclastics, basalts, and Urgonian, fossil-rich limestones. Except for the dykes, an analogous clast inventory is found in breccia beds dispersed within the sedimentary wedge, pointing to the breccia formation as extruded deposits discharged from the dykes. The dykes can be traced as cross-cutting the underlying Black Flysch strata for over 200 m; the clast composition implies their derivation from the lower Albian Monte Grande Formation (Agirrezabala, 2015; Fig. 4C). About 260 m below the level of seep carbonates and breccia, the Monte Grande Formation hosts a basaltic intrusion, ~600 m in diameter and 40 m in thickness (Table 1). The intrusion, referred to as the Larragan laccolith, resulted in syndepositional forced folding and peripheral fracturing of the overburden, creating pathways for the hydrocarbon seepage and sediment extrusion (Agirrezabala, 2015; Fig. 4C). The laccolith is accompanied by several sills protruding into sediments of the Black Flysch Group. Because of the limited exposure of the laccolith, the sills have been the main focus of previous studies of the influence of the Gorliz intrusion on its host succession (Agirrezabala et al., 2014). In addition to the intrusives, the Albian volcanism is recorded at Gorliz in the form of diatremes exposed to the south-west of the laccolith (Agirrezabala et al., 2017), penecontemporaneous with the seep deposit, and a horizon of pillow-lavas post-dating the seep.

3. MATERIAL

The analysed samples were powdered using a microscope-mounted microdrill. The Nd and C – O isotope analyses included a total of 36 and 30 samples, respectively. Most samples, including all carbonates from the Ispaster and Gorliz sites, represent microcrystalline textures. This reflects both the general dominance of this fabric at all the studied seeps, and high REE contents typical of micrite compared to other carbonate textures (for discussions see Jakubowicz et al., 2015, 2019). As a result, for most deposits micrite was the only phase voluminous enough to enable combined Nd and stable isotope measurements. The sole exceptions are isopachous cements from a relatively large void of the Alkolea deposit. In addition, two samples of blocky spar from Kardala, and a small micritic sample from Gorliz were subjected only to C and O isotope measurements.

To provide the context required to interpret the Nd isotope signatures of the seep carbonates, we analysed also three samples of the basaltic intrusions exposed at Gorliz: one from the main, Larragan laccolith, and two from its subsidiary sills (sills A and B in Fig. 4C), as well as a single sample of a calcite vein cross-cutting the sill A. In addition, to establish the background ε_{Nd} signal of coeval seawater-derived pore waters, we analysed a set of non-seep, phosphate and carbonate materials from the Basque-Cantabrian Basin. Due to its high resistance to diagenetic alteration, fish fluorapatite is the most commonly applied archive of past seawater Nd isotope signatures for post-Palaeozoic, subaerially-exposed marine successions (Martin et al., 2010; Tachikawa et al., 2017). Accordingly, our analyses included a sample of a fish jaw, collected from lower to middle Albian, outer-ramp marls ('Bermeo marls'; García-Mondéjar and Robador, 1986–87) cropping out at the northern margin of the basin, ~4 km north of the Bermeo village. These strata are not directly contemporaneous with the seep-hosting, upper Albian Black Flysch Group; no fish remains have, however, ever been found in this fossil-poor succession. Therefore, besides the mid-Albian fish material, we studied a set of micritic samples from a carbonate platform of the Urgonian Complex (Egino Formation;

Table 2
Sm-Nd, C and O isotope data of the studied Albian seep deposits and reference non-seep carbonate, phosphate and volcanic materials from the Basque-Cantabrian Basin.

Sample ID	Lithology	Weight (mg)	Sm (ppm)	Nd (ppm)	$^{147}Sm/^{144}Nd$	$^{143}Nd/^{144}Nd$ ($t = 0$)	$^{143}Nd/^{144}Nd$ ($t = 105$ Ma)	ε_{Nd} ($t = 105$ Ma)	$\delta^{13}C$ (‰ V-PDB)	$\delta^{18}O$ (‰ V-PDB)
Kardala seep deposit										
Ka-1a-1	micritic calcite	162.55	6.07	12.69	0.2893	0.512325 ± 10	0.512126	−7.36 ± 0.20	−11.68	−9.62
Ka-1a-2	micritic calcite	66.78	5.66	10.51	0.3258	0.512372 ± 10	0.512149	−6.91 ± 0.20	−3.46	−10.47
Ka-1b	micritic calcite	258.94	2.85	6.93	0.2488	0.512305 ± 10	0.512134	−7.19 ± 0.20	−16.97	−7.84
Ka-1c	micritic calcite	123.17	4.34	10.43	0.2514	0.512230 ± 10	0.512111	−7.64 ± 0.20	−13.63	−9.19
	micritic calcite: average (±1σ)							*−7.3 (±0.3)*	*−11.4 (±5.0)*	*−9.3 (±1.0)*
Ka-1Bl	blocky sparry calcite								−9.20	−9.58
Ka-2	blocky sparry calcite								−5.17	−9.80
Alkolea seep deposit										
Al-1a	micritic calcite	245.97	1.23	3.43	0.2173	0.512176 ± 11	0.512027	−9.29 ± 0.21	−13.13	−4.49
Al-2	micritic calcite	261.17	1.62	5.18	0.1896	0.512156 ± 10	0.512026	−9.31 ± 0.21	−25.07	−5.26
Al-3	micritic calcite	261.12	1.25	3.29	0.2301	0.512234 ± 10	0.512076	−8.33 ± 0.20	−26.37	−3.34
Al-4	micritic calcite	309.22	0.86	2.39	0.2169	0.512187 ± 10	0.512038	−9.08 ± 0.20	−8.61	−3.76
	micritic calcite: average (±1σ)							*−9.0 (±0.4)*	*−18.3 (±7.6)*	*−4.2 (±0.7)*
Al-3	isopachous sparry calcite (2nd generation)	109.51	0.06	0.29	0.1267	0.512214 ± 15	0.512127	−7.34 ± 0.29	2.84	−5.01
Al-3	isopachous sparry calcite (1st generation)	48.64	0.15	0.67	0.1308	0.512194 ± 15	0.512105	−7.77 ± 0.29	8.54	−1.92
Ispaster seep deposit										
Is-A1-1	micritic calcite	279.41	0.78	2.73	0.1737	0.512245 ± 13	0.512126	−7.36 ± 0.25	−26.92	−10.56
Is-A1-3	micritic calcite	56.27	3.25	10.90	0.1800	0.512230 ± 10	0.512106	−7.75 ± 0.20	−6.10	−10.60
Is-A-5	micritic calcite	165.51	1.80	6.18	0.1757	0.512184 ± 10	0.512063	−8.59 ± 0.20	−4.50	−10.69
Is-A-7	micritic calcite	178.47	1.07	3.38	0.1911	0.512161 ± 9	0.512030	−9.23 ± 0.18	−25.81	−10.73
Is-A-8	micritic calcite	155.3	0.90	3.12	0.1741	0.512179 ± 8	0.512059	−8.66 ± 0.16	−22.57	−10.65
Is-B4-10	micritic calcite	89.58	1.65	5.13	0.1945	0.512224 ± 10	0.512090	−8.05 ± 0.20	−7.56	−11.31
Is-B-13	micritic calcite	198.62	0.72	2.33	0.1883	0.512189 ± 14	0.512060	−8.65 ± 0.27	−20.60	−11.54
Is-B-14	micritic calcite	102.76	1.62	5.52	0.1775	0.512168 ± 10	0.512046	−8.92 ± 0.20	−4.91	−10.58
	micritic calcite: average (±1σ)							*−8.4 (±0.6)*	*−14.9 (±9.3)*	*−10.8 (±0.4)*
Gorliz seep deposit										
Go-S-1a	micritic calcite	29.38	4.22	13.26	0.1924	0.512159 ± 13	0.512027	−9.29 ± 0.25		
Go-S-1b	micritic calcite	155.7	1.51	5.34	0.1716	0.512125 ± 7	0.512007	−9.67 ± 0.14	−23.33	−9.64
Go-S-1c	micritic calcite	222.99	0.80	3.55	0.1363	0.512125 ± 10	0.512031	−9.21 ± 0.20	−25.20	−10.69
Go-S-1d	micritic calcite	56.65	2.85	12.88	0.1335	0.512120 ± 10	0.512028	−9.26 ± 0.20	−22.03	−9.29
Go-Sc-2a	micritic calcite	188.2	1.30	5.29	0.1490	0.512141 ± 9	0.512038	−9.07 ± 0.18	−32.09	−3.52
Go-Sc-2b	micritic calcite	192.32	0.83	3.62	0.1383	0.512139 ± 10	0.512044	−8.96 ± 0.20	−34.52	−3.01
MR 12c	micritic calcite	132	1.00	4.02	0.1500	0.512129 ± 10	0.512025	−9.30 ± 0.20	−24.56	−9.90
MR 13	micritic calcite	88.4	1.59	6.49	0.1476	0.512139 ± 10	0.512036	−9.08 ± 0.20	−29.39	−3.95
MR 20b	micritic calcite	141.19	0.64	2.94	0.1315	0.512100 ± 10	0.512009	−9.61 ± 0.20	−19.42	−10.35
MR 7	micritic calcite								−24.16	−9.76
MR 7	micritic calcite	130.16	1.16	4.69	0.1501	0.512100 ± 10	0.511996	−9.86 ± 0.20	−24.27	−8.95

	micritic calcite: average (±1σ)							*−9.3 (±0.3)*	*−25.9 (±4.4)*	*−7.9 (±2.9)*
Gorliz intrusive volcanics (Larragan laccolith system)										
Go-La-5	volcanics, main laccolith	32.54	10.53	64.54	0.0987	0.512723 ± 10	0.512656	2.98 ± 0.20		
Go-Sil-3	volcanics, sill B	32.01	13.58	64.07	0.1281	0.512715 ± 10	0.512627	2.42 ± 0.20		
Go-Sil-4	volcanics, sill A	29.61	8.49	53.27	0.0964	0.512700 ± 9	0.512634	2.56 ± 0.18		
Go-Sil-4-C	calcite vein in volcanics, sill A	110.29	0.97	5.06	0.1161	0.512690 ± 7	0.512610	2.10 ± 0.14		
Carbonate platform, Urgonian Complex (Egino Formation)										
EGI-1	micritic limestone, calcite	298.54	0.07	0.39	0.1173	0.512092 ± 10	0.512011		−9.60 ± 0.20	
EGI-2	fossiliferous wackestone-packstone, calcite	284.38	0.09	0.42	0.1235	0.512100 ± 6	0.512016		−9.51 ± 0.12	
EGI-3	fossiliferous wackestone-packstone, calcite	270.26	0.19	0.91	0.1268	0.512112 ± 10	0.512025		−9.33 ± 0.20	
	platform carbonates: average (±1σ)								*−9.5 (±0.1)*	
ANT-9	fish jaw fluorapatite (Bermeo marls)	1.019	0.83	0.91	0.1383	0.512108 ± 10	0.512016		−9.50 ± 0.20	

García-Mondéjar et al., 2004) located in the southern part of the basin, 7 km west of the Altsasu village, and coeval to the studied seeps. As demonstrated in several previous studies, micritic carbonates can provide a robust record of past seawater Nd isotope signatures where the use of phosphatic archives is not feasible, provided no anomalous late-diagenetic alteration pathways were involved (e.g., Fanton et al., 2002; Martin et al., 2010; Holmden et al., 2013; Belka et al., 2021). Indeed, the narrow clustering of Nd isotope data obtained for the platform carbonates and fish fluorapatite (Section 5.1) supports the primary character of the unradiogenic Nd isotope signature reconstructed for the Albian seawater of the Basque-Cantabrian Basin.

4. METHODS

The Nd – Sm isotope measurements were performed in the Isotope Laboratory of the Adam Mickiewicz University, Poznań, Poland, on a Finnigan MAT 261 multi-collector thermal ionization mass spectrometer. The powdered carbonate samples (29–309 mg each) were weighed into 50 ml centrifuge tubes, treated with weak (5%) ultra-pure acetic acid and left on a mechanical shaker for 24 h at room temperature following the selective-dissolution procedure recommended by Rongemaille et al. (2011). The obtained solutions were centrifuged to separate the acid-soluble fraction; each residue was washed, dried and weighed to determine the content of the non-leachable fraction. To remove potential fine acid-insoluble particles, the supernatant liquids were passed through a syringe filter with a 0.2 μm PTFE membrane. The filtered solutions were then equilibrated with a mixed $^{149}Sm-^{150}Nd$ tracer. Rare earth elements (REE) were stripped from the solutions using the Fe hydroxide co-precipitation method described by Fanton et al. (2002). The fish fluorapatite sample (~1 mg) was spiked and dissolved in concentrated nitric acid. The samples of the volcanics (~50 mg) were powdered, spiked and dissolved with HF/HNO_3 (5:1). Light REE were separated from matrix elements on 50 μl teflon columns filled with EICHROM TRU resin. Separation of Nd and Sm was performed on 2 ml columns packed with EICHROM Ln resin. Nd and Sm (loaded as phosphate) were measured on Re in a double filament configuration. Isotopic ratios were determined in a dynamic (Nd) and static (Sm) mode. During the course of this study, the AMES standard yielded $^{143}Nd/^{144}Nd = 0.512126 \pm 9$ (2σ mean of thirteen analyses). The $^{143}Nd/^{144}Nd$ ratios were normalized to $^{146}Nd/^{144}Nd = 0.7219$, and Sm isotope ratios to $^{147}Sm/^{152}Sm = 0.56081$. Total procedure blanks were < 40 pg for Nd and Sm. Nd isotope data have been reported in the standard ε notation:

$$\varepsilon_{Nd} = \frac{\left(\frac{^{143}Nd}{^{144}Nd}\right)_{sample} - \left(\frac{^{143}Nd}{^{144}Nd}\right)_{CHUR}}{\left(\frac{^{143}Nd}{^{144}Nd}\right)_{CHUR}} \times 10^4$$

where CHUR denotes the present-day Chondritic Uniform Reservoir ($^{143}Nd/^{144}Nd = 0.512638$ and $^{147}Sm/^{144}Nd = 0.1967$; Jacobsen and Wasserburg, 1980).

The concentrations of REE and barium (Ba) were determined by triple-quadrupole inductively coupled plasma

mass spectrometry (ICP-QQQ-MS) in the Hydrogeochemical Laboratory of the Adam Mickiewicz University. The measurements were carried out with an Agilent 8800 Triple Quad mass spectrometer on the same sample solutions used for the Nd – Sm isotope analyses. The spectrometer operated in a gas mode, with He flowing at 4.5 mL/min. All parameters were manually optimized to achieve the best signal intensity and stability. The MassHunter software for ICP-QQQ-MS (Agilent Technologies, Japan) was used to control the instrument and to process the data. The determinations by ICP-QQQ-MS were performed using calibration curves obtained from a diluted stock multi-element standard 100 µg mL^{-1} (VHG Labs, Manchester, USA). The reagents used were ultrapure, and the water was deionized to a resistivity of 18.2 MΩ cm in a Direct-Q®3 Ultrapure Water System apparatus (Millipore, France). Analytical quality control was verified by analyses of certified reference materials, viz. SPS-SW2 (Spectrapure Standards As, Oslo, Norway). The analytical errors for the certified solutions were ≤ 0.04 ppb for REE and 0.7 ppb for Ba. The detection limits were ≤ 0.0012 ppb for REE and 0.008 ppb for Ba. The REE contents have been normalized to Post-Archean Australian Shale (PAAS; McLennan, 1989). Europium anomalies [$(Eu/Eu^*)_{SN}$; SN = shale-normalized values] were calculated using the standard equation for quantifying elemental anomalies in REE patterns: $(Eu/Eu^*)_{SN} = 2(Eu)_{SN}/[(Sm)_{SN} + (Gd)_{SN}]$. Because of the anomalous behaviour of La in seawater, Ce anomalies were determined following an alternative, geometric equation recommended by Lawrence et al. (2006): $(Ce/Ce^*)_{SN} = (Ce)_{SN}/[(Pr)_{SN}]^2 * (Nd)_{SN}$. Light rare earth elements (LREE) are defined as La, Ce, Pr and Nd, middle rare earth elements (MREE) as Sm, Eu, Gd, Tb and Dy, and heavy rare earth elements (HREE) as Ho, Er, Tm, Yb and Lu. The relative MREE/HREE- and LREE/HREE-enrichments are quantified in the form of $(Gd/Yb)_{SN}$ and $(Nd/Yb)_{SN}$ values, respectively.

The carbon and oxygen isotope analyses were carried out in the Stable Isotope Laboratory of GeoZentrum Nordbayern, Friedrich-Alexander University Erlangen-Nürnberg, Germany. CO_2 was liberated for the measurements by treating the carbonate powders with 100% phosphoric acid at 70 °C with an automated Gasbench II device, and analysed using a Thermo-Fisher Delta V Plus mass spectrometer. The measured isotope ratios are shown in the standard δ notation in ‰ relative to the V-PDB standard. Accuracy of the measurements was controlled by analyses of laboratory standards calibrated to the international standards NBS19 ($\delta^{13}C = 1.95‰$, $\delta^{18}O = -2.20‰$), IAEA-CO9 ($\delta^{13}C = -47.3‰$) and NBS18 ($\delta^{18}O = -23.2‰$). The average reproducibility (1σ) was ± 0.05‰ for both $\delta^{13}C$ and $\delta^{18}O$.

5. RESULTS

5.1. Nd isotopes

The measured Nd isotope ratios, expressed as ε_{Nd} values and corrected for the age-related effect of ^{147}Sm decay, are given in Table 2 and illustrated in Figs. 6 and 7. Among the

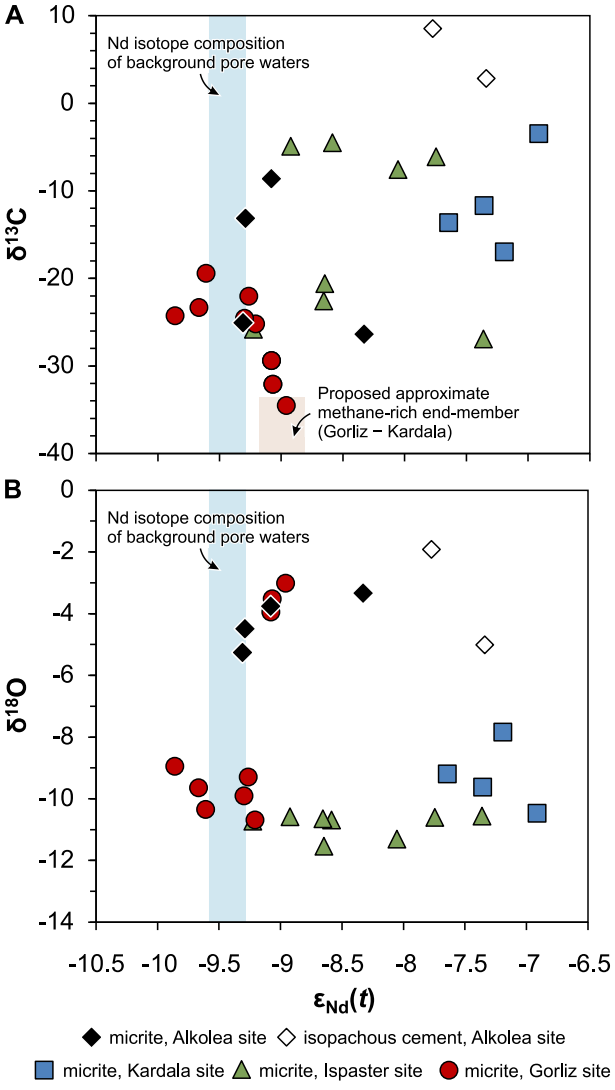

Fig. 6. Nd vs. C (A) and O (B) isotope cross-plots for the Albian seep carbonates of the Basque-Cantabrian Basin. The blue-shaded area corresponds to the range of ε_{Nd} values of coeval local marine pore waters inferred from non-seep carbonate and phosphate archives. (For interpretation of the references to colours in this figure legend, the reader is referred to the web version of this paper.)

seep carbonates, the most radiogenic signals have been observed in the Kardala deposit, with $\varepsilon_{Nd}(t)$ values falling within a relatively narrow range of −6.9 to −7.6. More moderate enrichment in ^{143}Nd, combined with considerably broader ranges of Nd isotope ratios, typifies the Alkolea and Ispaster carbonates, with their $\varepsilon_{Nd}(t)$ of −7.3 to −9.3 and −7.4 to −9.2, respectively. At Alkolea, the highest values were born by the two samples of isopachous sparry cements. The lowest $\varepsilon_{Nd}(t)$ values, clustering between −9.0 and −9.7, have been measured for the Gorliz deposit.

The intrusions exposed at Gorliz yielded high $\varepsilon_{Nd}(t)$ values, a feature generally characteristic of mafic igneous materials. The most radiogenic signatures have been observed for the main laccolith ($\varepsilon_{Nd}(t) = +3.0$). The associated sills A and

B show $\varepsilon_{Nd}(t)$ values of +2.6 and +2.4, respectively, and the single sample of vein calcite gave an $\varepsilon_{Nd}(t) = +2.1$. The inferred Albian background pore water signatures recorded in both the platform-carbonate and fish-phosphate archives consistently fall within a narrow cluster of unradiogenic $\varepsilon_{Nd}(t)$ values (−9.3 to −9.6 for the carbonates, and −9.5 for the phosphate).

5.2. Rare earth elements

As it is typical of seep carbonates, total REE concentrations (∑REE) measured in the analysed micrites are relatively high compared to typical normal-marine limestones. ∑REE range from 9.6 to 17.1 ppm for Gorliz, 9.8–14.8 ppm for Alkolea, 10.6–12.7 ppm for Ispaster, and 23.8–41.5 ppm for Kardala (Table 3). When normalised to PAAS, the REE patterns of these micrites consistently show pronounced enrichment in MREE [$(Gd/Yb)_{SN}$ ratios from 1.1 to as high as 2.1] and some LREE-depletion relative to HREE [$(Nd/Yb)_{SN} < 0.76$ for all deposits; Fig. 8]. Cerium anomalies, if present, are mostly minor. In addition, several samples display moderate enrichment in Eu [$(Eu/Eu^*)_{SN}$ of up to 1.4]. Barium concentrations range from 24.1 to 233.6 ppm.

The basaltic laccolith and its peripheral sill A bore high ∑REE (289.1–354.7 ppm) and REE patterns with general LREE-enrichment and strong positive Eu anomalies, all typical of mafic volcanics.

5.3. Stable isotopes

The measured C and O isotope ratios are consistent with more extensive stable isotope datasets reported in previous studies (Agirrezabala, 2009, 2015; Agirrezabala et al., 2013; Wiese et al., 2015; Supplementary Table 1). For the Kardala and Ispaster micrites and Alkolea isopachous cements, the heaviest $\delta^{13}C$ values observed here additionally extend the ranges documented to date (Fig. 5). Most samples gave $\delta^{13}C$ values conspicuously more negative than the signature of carbonates precipitating in equilibrium with coeval seawater ($\delta^{13}C = 1.5$ to 2.5‰; Jarvis et al., 2006). The ranges observed at individual seeps are broad. The lowest $\delta^{13}C_{micrite}$ values, ranging from −19.4 to −34.5‰, have been observed at Gorliz. The remaining deposits display more moderate ^{13}C-depletion, with $\delta^{13}C$ values between −4.5 to −26.9 for Ispaster, −8.6 to −26.4 for Alkolea, and −3.5 to −17.0 for Kardala micrites. The two samples of blocky cements from Kardala yielded $\delta^{13}C$ values of −5.2 and −9.2‰. The highest carbon isotope ratios documented in the present dataset have been observed in isopachous cements from the Alkolea deposit ($\delta^{13}C = 2.8$ and 8.5‰).

The measured $\delta^{18}O$ values are exclusively negative. The Kardala, Gorliz and Ispaster micrites show similar $\delta^{18}O_{min}$ values, but also marked differences in the data scatter, with their respective $\delta^{18}O$ ranges of −7.8 to −10.5‰, −3.0 to −10.7‰, and −10.6 to −10.7‰. Among the sparry phases, the blocky cements from Kardala gave $\delta^{18}O = -9.6$ and −9.8‰, whereas isopachous cements from Alkolea yielded values of −1.9 and −5.0‰.

6. DISCUSSION

A discussion on the sources of hydrocarbon-rich fluids emitted at the Albian seeps of the Basque-Cantabrian Basin must take account of the following constraints:

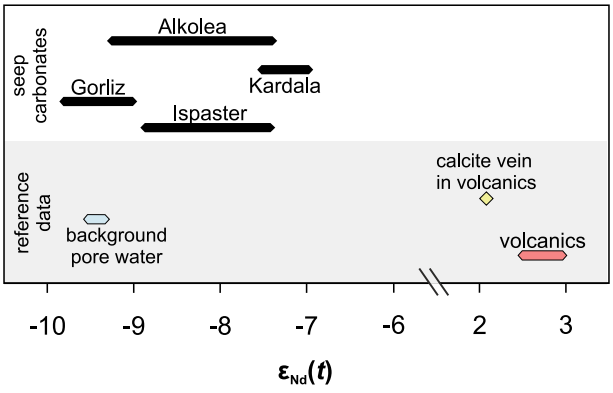

Fig. 7. Comparison of the ranges of Nd isotope ratios observed in the Albian seep deposits of the Basque-Cantabrian Basin, archives of the background pore water signal, and the igneous intrusion exposed in the basement of the Gorliz deposit.

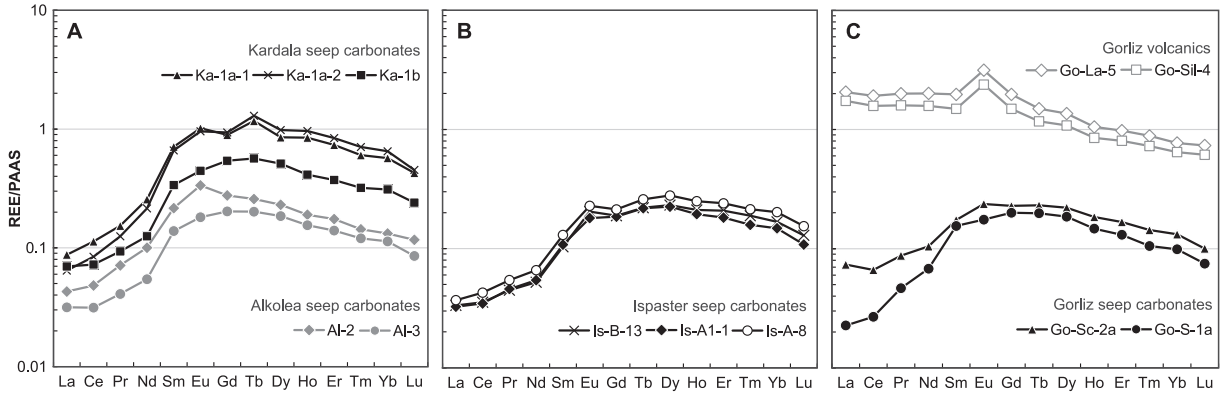

Fig. 8. PAAS-normalised REE patterns of the Albian micritic seep carbonates of the Basque-Cantabrian Basin (A: Kardala and Alkolea; B: Ispaster; C: Gorliz) and igneous intrusions underlying the Gorliz deposit (C).

Table 3
REE and Ba concentrations of the studied Albian seep carbonates and intrusive volcanics of the Basque-Cantabrian Basin.

Sample ID*	Element contents (ppm)														ΣREE	$(Ce/Ce^*)_{SN}$	$(Eu/Eu^*)_{SN}$	$(Gd/Yb)_{SN}$	$(Nd/Yb)_{SN}$
	La	Ce	Pr	Nd	Sm	Eu	Gd	Tb	Dy	Ho	Er	Tm	Yb	Lu	Ba					
Kardala seep deposit																			
Ka-1a-1a	3.35	9.01	1.35	8.69	3.94	1.10	4.16	0.90	3.98	0.84	2.10	0.24	1.61	0.18	233.56	41.46	1.23	1.27	1.57	0.45
Ka-1a-2	2.46	6.69	1.10	7.28	3.67	1.03	4.36	1.00	4.59	0.95	2.39	0.29	1.83	0.20	37.48	37.85	1.15	1.20	1.44	0.33
Ka-1b	2.66	5.76	0.82	4.24	1.87	0.48	2.52	0.44	2.40	0.41	1.06	0.13	0.87	0.10	193.55	23.78	1.04	1.01	1.74	0.40
Alkolea seep deposit																				
Al-2	1.64	3.84	0.63	3.40	1.20	0.36	1.29	0.20	1.08	0.19	0.50	0.06	0.37	0.05	54.34	14.79	0.95	1.36	2.09	0.76
Al-3	1.21	2.50	0.36	1.84	0.77	0.20	0.94	0.16	0.87	0.15	0.40	0.05	0.32	0.04	62.38	9.80	1.02	1.06	1.79	0.48
Ispaster seep deposit																				
Is-A1-1	1.24	2.76	0.40	1.84	0.60	0.19	0.86	0.17	1.05	0.19	0.52	0.06	0.42	0.05	186.37	10.36	0.90	1.23	1.25	0.37
Is-A-8	1.41	3.40	0.48	2.23	0.72	0.25	0.99	0.20	1.30	0.25	0.68	0.09	0.57	0.07	213.80	12.65	0.95	1.33	1.05	0.33
Is-B-13	1.28	2.82	0.40	1.77	0.57	0.22	0.88	0.17	1.09	0.21	0.59	0.08	0.47	0.06	71.38	10.60	0.92	1.40	1.12	0.31
Gorliz seep deposit																				
Go-S-1a	0.87	2.14	0.41	2.30	0.86	0.19	0.93	0.15	0.87	0.15	0.37	0.04	0.28	0.03	24.15	9.59	0.84	0.99	2.02	0.69
Go-Sc-2a	2.81	5.28	0.77	3.55	0.97	0.26	1.07	0.18	1.03	0.18	0.48	0.06	0.37	0.04	30.82	17.05	0.91	1.18	1.73	0.79
Gorliz intrusive volcanics (Larragan laccolith system)																				
Go-La-5	78.76	152.43	17.64	68.13	10.93	3.40	9.18	1.16	6.37	1.04	2.79	0.36	2.17	0.32	332.56	354.68	0.96	1.60	2.56	2.61
Go-Sil-4	66.46	125.71	14.09	53.55	8.28	2.57	6.95	0.91	5.06	0.84	2.29	0.29	1.82	0.27	347.93	289.10	0.98	1.60	2.31	2.44

*For lithological information see Table 2.

1) For three out of four studied seeps, the $\varepsilon_{Nd}(t)$ values of methane-seep carbonates are notably higher than the reconstructed Nd isotope signature of background, seawater-derived pore waters;
2) The single, Gorliz deposit stands out by its significantly less pronounced involvement of radiogenic Nd, displaying $\varepsilon_{Nd}(t)$ values largely overlapping with the background pore water range. This deposit shows also other distinguishing characteristics: the smaller number and size of carbonate bodies, scarcity of chemosynthesis-dependent biota, and its spatial association with a forced fold and former sediment extrusions;
3) All seeps of the Basque-Cantabrian area were apparently underlain by mafic igneous intrusions, either observed directly in outcrops (Gorliz), or imaged seismically (Ispaster, Kardala-Alkolea). While sharing a similar age, genesis and geotectonic setting, these intrusions show also differences in their geometries, host rocks, and emplacement depths.

Altogether, these observations place constraints on the processes responsible for the methane formation and expulsion in the Basque-Cantabrian rift, at the same time offering field-based clues pertinent to verification of general, largely theoretical models of hydrocarbon generation by igneous intrusions.

6.1. Isotopic record of magmatic-influenced fluids in the Basque-Cantabrian Basin: general constraints

The Nd isotope system belongs to the most important tracers of interactions between solid and dissolved phases in hydrogeological systems (Piepgras and Wasserburg, 1980; Lacan and Jeandel, 2005; Tachikawa et al., 2017). The merit of the method lies in the combination of the short residence time of Nd in seawater, no Nd isotope fractionation during biological or near-surface mineral precipitation processes, and marked differences in Nd isotope composition of different crustal materials. Rocks derived from depleted-mantle sources, i.e., mafic igneous rocks, show conspicuous enrichment in the radiogenic isotope ^{143}Nd (high ε_{Nd} values, up to +13), whereas the continental crustal materials, such as felsic igneous rocks and siliciclastic sediments derived from their weathering, reveal strong ^{143}Nd-depletion (ε_{Nd} values of down to −20; Shaw and Wasserburg, 1985; Goldstein and Jacobsen, 1988). These differences are partially inherited by fluids during fluid-rock interactions. Much focus in recent Nd isotope studies has been placed on determination of lithological controls on the spatial variability of seawater ε_{Nd} values (e.g., Arsouze et al., 2007; Horikawa et al., 2011; Fröllje et al., 2016). One important aspect of these investigations has been a better understanding of the role that fluid-rock interactions play in shaping Nd isotope signatures of shallow-level interstitial waters (Abbott et al., 2015; Du et al., 2016; Blaser et al., 2019). This has also reinvigorated interest in the use of Nd isotopes as a proxy of fluid circulation at submarine fluid emissions, including not only mid-ocean ridge-related hydrothermal vents, for which Nd has tradi-

tionally been applied (e.g., Piepgras and Wasserburg, 1985; Stichel et al., 2018; Chavagnac et al., 2018), but also sediment-hosted fluid discharges.

Studies of the sediment-hosted fluid discharges hold particular promise, as the complex fluid sources typical of such settings, differentially affecting different geochemical systems, encourage combined use of various isotope tracers. Because of the mainly terrigenous control on the seawater Nd budget, for most oceanic basins shallow-burial, seawater-derived pore waters show unradiogenic ε_{Nd} values (a global seawater $\varepsilon_{Nd\text{-average}} = < -8$; Tachikawa et al., 2017). Accordingly, most methane-seep carbonates, precipitating shallowly below the sediment–water interface, can be expected to record correspondingly seawater-like, unradiogenic ε_{Nd} signals. Indeed, low ε_{Nd} values close to ambient seawater have been observed in the few Nd isotope studies performed at modern seeps (Bayon et al., 2011; Freslon et al., 2014). Where deviations from seawater signatures were, in turn, reported for Cenozoic seeps, they were towards more unradiogenic ε_{Nd} values (Ge et al., 2020). The enrichment of seep carbonates in radiogenic Nd provides, therefore, an important indication of a presence in the plumbing system of mafic, volcanic-derived materials. Indeed, increased $\varepsilon_{Nd}(t)_{carbonate}$ values have been documented for fossil seeps overlying volcanic successions from a passive margin (Jakubowicz et al., 2015), sedimented rift (Jakubowicz et al., 2019) and subduction zone (Jakubowicz et al., 2020). In addition, advection of deep-seated fluids with exotic ε_{Nd} signatures has been considered as a source of some ^{143}Nd-enrichment observed in sedimentary organic matter at seeps of the Eastern Mediterranean Sea (Freslon et al., 2014).

Shallow-level igneous intrusions are typical elements of sedimented spreading systems (Einsele, 1980; Planke et al., 2005; Lizarralde et al., 2011; Angkasa et al., 2017). A causal link between the magmatism and formation of hydrocarbons has been documented for many of such rifts, including both modern (Guaymas Basin, Okinawa Trough, Sea of Japan, Middle Valley of the Juan de Fuca ridge) and fossil (e.g., Paleocene-Eocene North Atlantic region) examples (e.g., Welhan and Lupton, 1987; Svensen et al., 2004; Cruse and Seewald, 2006; Kawagucci et al., 2013; Snyder et al., 2020). Analogously, a similar relationship appears suggested for the Basque-Cantabrian rift by the spatial association between the studied methane-seep deposits and intrusive bodies, and the coincidence between the methane seepage and the mid-Cretaceous peak of igneous activity in this area. Indeed, fluid-rock interactions involving mafic igneous materials have been recorded to various degrees by the Nd isotope composition of all the Basque seep deposits. For three out of four analysed seeps, the involvement of the radiogenic Nd source is very distinct, with the highest recorded $\varepsilon_{Nd}(t)_{carbonate}$ values being from ~2.5 (Kardala deposit) to ~2 (Ispaster and Alkolea deposits) ε_{Nd} units higher than the background pore water signal. The contribution of volcanogenic Nd is most evident for the Kardala locality, where even the least radiogenic $\varepsilon_{Nd}(t)_{carbonate}$ value is still nearly 2 ε_{Nd} unit higher than the mean background signature. The least pronounced ^{143}Nd-enrichment, not exceeding 0.3 ε_{Nd} unit, is observed at Gorliz. For Alkolea and Ispaster, the $\varepsilon_{Nd}(t)_{carbonate}$ values vary from relatively radiogenic ratios to signals close to the range of non-seep pore waters.

Similarly broad scatters of Nd isotope data have been recorded for other seeps hosted by magmatism-affected basins (Jakubowicz et al., 2015, 2019, 2020). Generally, in such areas the expression of deep, volcanogenic fluid components is strongly dependent on the high spatial and temporal variability in fluid composition and flow rates, inherent to seepage-affected interstitial waters (cf., Himmler et al., 2010; Birgel et al., 2011). Accordingly, the range of ε_{Nd} values observed at the studied Basque seeps can be understood primarily in the context of mixing between background pore waters and deep fluids enriched in ^{143}Nd. In marine settings, the shallow-burial pore water REE inventories, and thus Nd isotope signatures, are typically dominated by reduction of marine-derived, authigenic Fe-Mn oxides, and hence usually resemble local seawater signal (Gutjahr et al., 2007; Molina-Kescher et al., 2014). As a consequence, where no exotic Nd supply by fluid advection is involved, the offset between deep seawater and shallow-level pore water very rarely exceeds 1 ε_{Nd} unit. Indeed, the most significant offsets, still not larger than 1–1.5 ε_{Nd} units, have been recorded for pore water profiles typified by exceptional abundance of volcanic ash dispersed within the sediment (Abbott et al., 2015). Given the infilling of the Basque-Cantabrian Basin with the thick siliciclastic succession, with its inherent unradiogenic Nd isotope composition, background pore waters do not provide, therefore, a likely source of the ^{143}Nd-rich fluids involved in precipitation of the studied seep carbonates. In the four investigated sections, the turbiditic sediments underlying the seep deposits do not contain volcaniclastic particles, and volcaniclastics layers identified at some sections (Agirrezabala and García-Mondéjar, 2001) are invariably very rare and thin (<2 cm in thickness). Accordingly, the fish sample used here as an archive of the background pore water signature yielded a relatively unradiogenic ε_{Nd} value, within the range defined by the platform carbonates. In this context, the igneous intrusions present in the basements of the studied seeps constitute the most plausible source of the excess ^{143}Nd available in the Basque-Cantabrian Basin at the time of hydrocarbon seepage.

6.2. Site-specific patterns in geochemical signatures of fluid sources

6.2.1. Kardala and Gorliz sites

In the spectrum of the observed isotopic signatures, the Kardala and Gorliz deposits appear to represent two end-member cases of a relative role of the volcanogenic fluid component. Both these seeps are defined by comparatively narrow ranges of $\varepsilon_{Nd}(t)$ values, which do not overlap: the lowest $\varepsilon_{Nd}(t)$ value observed at Kardala is nearly 1.5 ε_{Nd} units higher than the highest $\varepsilon_{Nd}(t)$ value measured for the Gorliz deposit. Similarly, the carbon isotope ratios of the early-diagenetic carbonates from the two sites define mostly distinct ranges, with the Gorliz carbonates showing, on average, considerably more pronounced ^{13}C-depletion. Furthermore, for both deposits, there are consistent varia-

tions within the C – O and Nd – C isotope datasets. In carbonate systems, the presence of co-variance patterns between different isotopic systems can result from three processes: (1) mixing between distinct fluid end-members upon carbonate precipitation; (2) involvement of different generations of carbonate cements; and (3) diagenetic alteration affecting isotopic proxies with similar sensitivity to post-depositional overprint.

In any study devoted to ancient carbonates, a role of diagenesis must be evaluated first. Among isotopic systems commonly used in studies of carbonate rocks, Nd isotopes belong to those least prone to diagenetic alteration. Shifting the primary $\varepsilon_{Nd}(t)$ values requires very high fluid-rock ratios, which are not attainable in most feasible alteration pathways during marine-burial diagenesis (cf., Banner and Hanson, 1990; Webb et al., 2009; Liu et al., 2019). Of greatest importance here are the low REE contents typical of most late-diagenetic solutions, while seep carbonates are typically characterized by high primary REE concentrations, which makes them particularly resistant to shifts in their ε_{Nd} values (see Jakubowicz et al., 2015 for a discussion). Accordingly, the conspicuous MREE-enrichment ('REE-bulge') observed in the shale-normalised REE-patterns of the studied deposits is characteristic of primary seep carbonates (cf., Himmler et al., 2010; Birgel et al., 2011; Jakubowicz et al., 2015; Argentino et al., 2019). This type of REE distribution reflects their precipitation from very early-burial pore fluids, and thus under major REE release from reduction of, inherently MREE-enriched, Fe-Mn oxides (cf., Haley et al., 2004). On the other hand, it is markedly different from typical patterns observed in deeper-burial pore fluids (Haley et al., 2004; Kim et al., 2012; Zwicker et al., 2018). Interestingly, the presence of some positive Eu anomalies, observed in most analysed samples, is a typical feature of fluids affected by elemental exchange with mafic igneous rocks (Douville et al., 1999). For the Basque seeps, this may further hint at a role of fluid interactions with the intrusive volcanics. The anomalies are, however, relatively small, and for many samples their conclusive interpretation is hampered by the apparent effect of the Gd-depletion, as well as, in some cases, the increased Ba concentrations, the latter causing potential artifacts during ICP-MS measurements (Dulski, 1994). Of importance may have also been the very strongly reducing conditions developing at seeps, which may produce pore water Eu-enrichment with no involvement of fluid interactions with igneous materials (Jakubowicz et al., 2015 and references therein).

While the C isotope system shows comparatively low susceptibility to diagenetic alteration, it is less resistant to advanced diagenesis (Banner and Hanson, 1990; Marshall, 1992; Knauth and Kennedy, 2009). In such cases, the high fluid-rock ratios required result, however, typically in pervasive recrystallization of the original carbonate fabrics; this is not observed for the studied carbonate samples, which show generally good preservation of the original textural features. Furthermore, the measured, negative $\delta^{13}C$ values are typical of fossil seep carbonates (Peckmann and Thiel, 2004; Campbell, 2006; Jakubowicz et al., 2017). Distinguishing between the primary vs. diagenetic origin of these signals can be further aided with analysis of their co-variance relationships with different isotopic systems. The large stable isotope datasets collected in the present and previous studies (Agirrezabala et al., 2013; Agirrezabala, 2015) depict consistent, negative correlations between the $\delta^{13}C$ and $\delta^{18}O$ data for both Kardala and Gorliz deposits (Fig. 5). Because oxygen is much more prone to diagenetic exchange, resetting $\delta^{18}O_{carbonate}$ values typically takes place notably before alteration of the more diagenetically-resistant isotopic proxies, such as $\delta^{13}C$ and ε_{Nd} signatures (Banner and Hanson, 1990; Jaffrés et al., 2007; Knauth and Kennedy, 2009). Consequently, diagenetic re-equilibration of the oxygen isotope system most commonly results in narrow clustering of $\delta^{18}O$ data. Conversely, a broad range of $\delta^{18}O$ values and their correlation with different, less alteration-prone isotope proxies support a low level of alteration of the archived isotope data (Banner and Hanson, 1990). While it is likely that the oxygen isotope ratios in individual samples could have been shifted to some extent, the general preservation of the linear $\delta^{13}C - \delta^{18}O$ co-variances provides a strong argument for the mostly primary nature of the carbonate $\delta^{13}C$ and $\delta^{18}O$ values. For our $\delta^{13}C$ data, this is further supported by their correlation with the $\varepsilon_{Nd}(t)$ signals, especially for the Gorliz deposit.

When analysed together, the isotopic systematics of the Gorliz and Kardala carbonates can be to a large degree explained in terms of mixing between two cement end-members. The first, ^{13}C-depleted component is similar for both sites. If treated as hypothetical mixing patterns, the trends emerging from the $\delta^{13}C - \delta^{18}O$ data would point to a shared cement end-member having $\delta^{18}O$ within a few per mil of zero, and $\delta^{13}C$ in the range of −35 to −40‰. As far as it can be judged from the limited number of the Nd measurements available for Kardala, the $\delta^{13}C - \varepsilon_{Nd}(t)$ dataset shows a consistent pattern with a shared ^{13}C-depleted end-member. Therefore, we suggest that, although representing two separate hydrocarbon systems, the methane-rich endmembers at both Kardala and Gorliz were geochemically similar and characterised by the combination of moderately negative $\delta^{13}C$, high $\delta^{18}O$, and relatively unradiogenic ε_{Nd} values. This cement end-member can be interpreted as precipitated mostly from fluids representative of a relatively shallow, outer parts of the thermal aureoles produced by the intrusions, where thermogenic methane generation was at its most intense, and enrichment in volcanic-derived ^{143}Nd was less pronounced.

The second cement end-members recorded at Kardala and Gorliz show, on the one hand, similarities in their $\delta^{18}O$ values, but, on the other hand, clear differences in their $\delta^{13}C$ and, in particular, $\varepsilon_{Nd}(t)$ signals. Conclusive interpretation of the significant ^{18}O-depletion shared by the ^{13}C-enriched end-members at both sites is problematic, as it is also for analogously ^{18}O-depleted seep carbonates hosted by modern rifts (e.g., Núñez-Useche et al., 2018). Agirrezabala (2009, 2015) interpreted the low $\delta^{18}O_{carbonate}$ values typifying the Cretaceous Basque seeps as indicative of their increased precipitation temperature. This interpretation is particularly well supported for the $\delta^{18}O$ data of blocky calcites and saddle dolomites, precipitated during

progressive burial and representing fabrics expected to have been stable throughout diagenesis. Nevertheless, for Kardala even the isotopically heaviest of the early-diagenetic carbonates still show pronounced depletion in ^{18}O. For the most ^{18}O-depleted micritic samples, their $\delta^{18}O$ values would translate into precipitation temperatures of over 60 °C (cf., Friedman and O'Neil, 1977; Agirrezabala, 2009). These would have most likely been attained at depth below the sediment–water interface. In general, the occurrence of the Kardala and Gorliz carbonates as predominantly small, scattered micritic concretions is indicative of their precipitation from sediment pore waters in the relatively deep sulphate-methane transition zone (cf., Peckmann et al., 2009). These palaeotemperature estimates do not, therefore, provide direct constraints on the habitat characteristics of the seafloor-dwelling seep communities. An alternative explanation for the presence of the $\delta^{18}O - \delta^{13}C$ correlation would be a major influx of meteoric fluids; this possibility appears, however, implausible given the palaeoenvironmental setting of the studied seeps (Agirrezabala, 2009), and the trend towards decreasing $\delta^{18}O_{carbonate}$ values with progressive burial, suggestive of a deep-seated origin of the precipitation fluids. Finally, low $\delta^{18}O_{fluid}$ values may also develop in pore waters affected by relatively low-temperature basalt alteration to smectite (Lawrence et al., 1979; Lawrence and Gieskes, 1981). The potential of such processes to result in significant fluid ^{18}O-depletion in systems with dynamic fluid flow remains, however, insufficiently understood. At temperatures > 60 °C, smectite dehydration, rather than smectite formation, becomes a dominant silicate weathering process, releasing fluids with high $\delta^{18}O$ values, expulsion of which has been well documented for some convergent margins (Dählmann and de Lange, 2003; Hensen et al., 2004). The involvement of basalt alteration in the ^{18}O-depletion observed in the Basque seep carbonates would, therefore, require a significant degree of intrusion cooling at the time of the fluid seepage. Such an interpretation is further complicated by the temperature constraints of thermogenic hydrocarbon formation (see Section 6.3), as well as the combination of low $\delta^{18}O$ and $\varepsilon_{Nd}(t)$ values observed in the Gorliz deposit.

Besides the different level of ^{13}C-depletion, the most significant difference between the second, ^{13}C-depleted cement end-members recorded at Kardala and Gorliz is in their contrasting $\varepsilon_{Nd}(t)$ values. Whereas at Kardala the most ^{13}C-enriched and ^{18}O-depleted samples show pronounced enrichment in ^{143}Nd, for Gorliz the trend is towards decreasing, rather than increasing $\varepsilon_{Nd}(t)$ values with increasing $\delta^{13}C$ and decreasing $\delta^{18}O$ (Fig. 6). For Kardala, the ε_{Nd}-$\delta^{13}C$ relationship can be explained in terms of the zonation of fluid release patterns expected for contact aureoles, with the zone directly adjacent to the intrusion-sediment contact producing the most ^{143}Nd-enriched fluids, but not favourable for hydrocarbon generation due to the temperature constraints. Possibly, this may include also some contribution of radiogenic Nd from fluids derived directly from intrusion devolatilisation (cf., Schutter, 2003), and hence devoid of hydrocarbons. For Gorliz, the ^{13}C-enriched cement end-member apparently precipitated from fluids with lower, although still significant, contribution of hydrocarbons, and no detectable input of volcanogenic Nd. This points to a distinct, apparently less evolved character of the second end-member recorded at Gorliz, which can be attributed to the shallower depth from which these interstitial fluids originated, and a different mechanisms and rate of fluid discharge triggered by the Gorliz intrusion. When combined with the overall much lower $\varepsilon_{Nd}(t)_{carbonate}$ values observed at Gorliz, the disparate patterns in the ε_{Nd}-$\delta^{13}C$ systematics of the Gorliz and Kardala deposits have broader bearing on the nature of igneous control on fluid expulsion at these sites and will be discussed in detail in Section 6.4.

6.2.2. Ispaster and Alkolea sites

For the Ispaster and Alkolea deposits, interpretation of the isotope data is more difficult, because there are no distinct correlation trends among the different systems. In sedimented rifts, the chemistry of emitted fluids is strongly modified by their interactions with sediments during both the recharge and discharge circulation stages (Piepgras and Wasserburg, 1985; Seewald et al., 1994; Cruse and Seewald, 2006; Kawagucci et al., 2013). Because of the differential behaviour of different elements during such interactions, this can result in various degrees of decoupling between different isotopic proxies. Modification of the original, deep fluid signatures during subsequent seepage appears particularly likely for the complex geochemical systematics recorded at Alkolea, for which special local constraints were probably involved (see Section 6.3). For fossil seeps, the primary geochemical variability can be additionally obscured by effects of later diagenesis. Of particular note for the Ispaster carbonates are their relatively narrowly clustered, strongly negative $\delta^{18}O$ values. This is a common characteristic of diagenetically-altered carbonates, reflecting pervasive overprinting of original signatures with those of diagenetic fluids (Banner and Hanson, 1990). Accordingly, for Ispaster this pattern has been attributed to diagenetic alteration by Agirrezabala et al., (2013). The clustering of $\delta^{18}O$ values does not automatically imply that $\delta^{13}C$ values have been altered as well (cf., Banner and Hanson, 1990), given that, because of the high variability of environmental conditions at seeps, the range in the primary carbon isotope ratios of seep deposits may be very broad (Peckmann and Thiel, 2004; Campbell, 2006). For Ispaster, some diagenetic shifts of the original carbon isotope signatures might be suggested by the particularly broad range of the $\delta^{13}C_{carbonate}$ values, much broader than these observed at Gorliz and Kardala, and close to both these deposits combined. At the same time, however, this large scatter is accompanied by the analogously broad variability of the ε_{Nd} values, which are much less susceptible to diagenetic alteration, attesting to the primarily increased isotope variability of cements involved in the Ispaster deposit. Conversely, assuming that the variability of the $\varepsilon_{Nd}(t)_{carbonate}$ values reflects partial resetting of the Nd isotope system would require $\delta^{13}C_{carbonate}$ values to have been reset notably earlier, resulting in their narrow clustering (cf., Banner and Hanson, 1990). This seems to suggest that, rather than isotopic re-equilibration of previously precipitated carbonates, the C and Nd isotope signatures of the

Ispaster micrites record increased contribution of later-diagenetic cements, a scenario consistent with the relative enrichment of the Ispaster carbonates in HREE (low $[Gd/Yb]_{SN}$ ratios; Table 3), a feature common for pore fluids below the zone of Fe-Mn oxide reduction in which seep carbonates typically form (Kim et al., 2012; Zwicker et al., 2018).

6.3. Thermogenic vs. biogenic origin of hydrocarbons

The enrichment of the studied Basque seep carbonates in radiogenic, apparently volcanic-derived Nd is in accord with several lines of structural, petrological and geochemical arguments presented in previous studies (Agirrezabala, 2009, 2015; Agirrezabala and Dinarès-Turell, 2013; Agirrezabala et al., 2013, 2014), pointing to the igneous intrusions as the main trigger of the Albian hydrocarbon generation in the Basque-Cantabrian rift. Further constraints on the magmatic role in the methane formation are placed by the relatively high $\delta^{13}C$ values of the seep deposits, not lower than −27‰ for the Kardala, Alkolea and Ispaster sites, and only to −39‰ for Gorliz. Such signatures are most typical of carbonates formed due to oxidation of thermogenic methane (e.g., Peckmann and Thiel, 2004; Orphan et al., 2004; Naehr et al., 2007). The broad range of the observed $\delta^{13}C_{carbonate}$ values can be primarily accounted for by mixing between carbon derived from the thermogenic methane, with its typically moderate level of ^{13}C-depletion ($\delta^{13}C = -20$ to −50‰; Whiticar, 1999), and isotopically heavier carbon supplied from background pore waters ($\delta^{13}C \approx 0$‰). The thermogenic source of hydrocarbons is further supported by the presence in the Kardala, Alkolea and Ispaster deposits of the pyrobitumen infills, since only thermogenic alteration of organic matter results in the formation of significant quantities of longer-chain hydrocarbons and solid bituminous residues that accompany methane (e.g., Simoneit et al., 1988; Whiticar, 1999). Compared to methane, migration of such heavy hydrocarbons may be hampered, and their solidification can take place already in the subsurface (cf, Simoneit et al., 1988; Sturz et al., 1996), in line with the later appearance of the pyrobitumens in the paragenetic sequence. Furthermore, the pyrobitumens are directly pre-dated by saddle dolomite, comprising a well-established geothermometer indicative of precipitation temperatures of > 60 °C (Machel, 2004), consistent with thermogenic formation of hydrocarbons through catagenesis (Tissot and Welte, 1978). Notably, at Alkolea the saddle dolomite is followed by the association of sulphate and carbonate minerals indicative of their shallow-burial hydrothermal origin (Agirrezabala, 2009).

For the studied seeps, the thermogenic origin of hydrocarbons requires involvement of the intrusive magmatism. Agirrezabala et al. (2008) provided geochemical evidence that the pyrobitumens found in the Basque seep deposits were sourced from the underlying Black Flysch Group. Because the thickness of these sediments does not exceed 1 km for any of the studied sites, in the absence of igneous activity no feasible geothermal gradients would be conducive to thermogenic hydrocarbon generation, given that catagenetic oil production is initiated at ~60 °C, and most methane forms at > 100 °C (Tissot and Welte, 1978; Stolper et al., 2014). In thermal aureoles of igneous intrusions, development of temperatures sufficient for catagenesis can, in turn, be considered geologically instantaneous (Simoneit, 1994), and is accompanied by abrupt overpressure build-up and host rock fracturing, favouring rapid fluid expulsion (Schutter, 2003; Jamtveit et al., 2004; Iyer et al., 2017). Accordingly, Agirrezabala et al. (2014) documented contact metamorphic effects of a sill underlying the Gorliz deposit, including metamorphic mineral assemblages indicative of temperatures exceeding 600 °C at the intrusion contact and 200 °C at 55% intrusion thickness, and the presence in the aureole of abundant bituminous residues left after pyrolytic methane release. Likewise, the extensive Nd isotope exchange between the fluids and the volcanics has been recorded in the present contribution as the very high $\varepsilon_{Nd}(t)$ value of the sill-hosted calcite veins. Most likely, this reflects calcite precipitation from CO_2 generated by the sediment heating, because fluids generated by thermal alteration of organic-rich argillites are typically dominated by CH_4 and CO_2 (cf., Seewald et al., 1994; Aarnes et al., 2010; Agirrezabala et al., 2014).

In addition to thermogenic hydrocarbons, an involvement of an additional, biogenic methane source may explain some of the geochemical characteristics observed in the Alkolea deposit. Of particular note here is the remarkably broad range of the reported $\delta^{13}C$ values, spanning in total 50‰ (Table 2 and Supplementary Table 1), and the presence of the exceptionally high, positive $\delta^{13}C$ values measured in two samples of the isopachous cement. The presence of such ^{13}C-enriched carbonates is most typical of seeps issuing biogenic, rather than thermogenic methane, where they incorporate carbon derived from residual, exceptionally ^{13}C-enriched CO_2 produced during microbial methanogenesis (cf., Tissot and Welte, 1978; Whiticar, 1999). This is combined with the presence of early isopachous cements with some of the lowest $\delta^{13}C$ values known from the studied Basque seeps (−41.5‰; Agirrezabala, 2009). These characteristics may suggest that the Alkolea seep expelled hydrocarbons of mixed origin, including a contribution from biogenic methane, with its typically lower $\delta^{13}C$ values (Whiticar, 1999). Most studied buried rifts host emissions of both thermogenic and biogenic methane, and seeps discharging mixtures of both hydrocarbon sources are relatively common in these settings (Cruse and Seewald, 2006; Kawagucci et al., 2013; Geiler et al., 2018; Teske et al., 2019). Such a scenario may account for both the large scatter of the C and Nd isotope data, and the moderately negative $\delta^{18}O$ values of the Alkolea carbonates. The latter, the highest among the studied Basque seeps and suggesting a comparatively low temperature of the seeping fluids, are consistent with increased mixing with shallower-level fluids. Notably, the methanogenesis-related cements show a pronounced enrichment in volcanogenic Nd, implying, together with the presence of the relatively late-diagenetic hydrothermal minerals, that the advection of the volcanic-influenced fluids continued through progressive burial of the seep deposit. The combination of the heavy carbon isotope composition and the particularly high degree of this

^{143}Nd-enrichment can be explained by the different sources dominating C and Nd isotope budgets at different depths in the sediment pore waters. Because anaerobic oxidation of methane takes place at a relatively shallow depth, requiring continuous recharge of sulphate-bearing seawater, the ε_{Nd} signature of the seeping fluids is partially obscured in seep carbonates by the relatively intense supply of Nd with seawater-like isotope signature. Below the zone of methane oxidation, in turn, contribution of seawater-derived REE decreases with depth, and interstitial waters in the methanogenesis zone typically show very low REE concentrations (Kim et al., 2012; Soyol-Erdene and Huh, 2013). Since the absence of sulphate in this zone precludes also release of methane-derived carbon to the dissolved inorganic carbon pool, methanogenesis can, therefore, be expected to affect the δ^{13}C signal of the seeping, volcanic-influenced fluids much more readily than their ε_{Nd} values. Overall, the apparently higher complexity of fluid sources at Alkolea compared to the nearby Kardala site may have been associated with its more complex structural and facies context. For the Kardala seep, its direct association with the Laugarren Hondartza-Mutriku fault was likely responsible for its particularly pronounced record of the deep, ^{143}Nd-enriched fluid signature. For Alkolea, on the other hand, the presence of the two angular unconformities, as well as the breccia horizon underlying the seep deposit may have favoured mixing of fluids originating from both deep and shallow sources, entailing increased variability of geochemical systematics recorded in its authigenic precipitates.

6.4. Divergent responses to different styles of intrusion emplacement

Interestingly, the Gorliz seep, representing the sole site for which the intrusive volcanics can be observed in outcrops, rather than in seismic images, shows also the lowest contribution of volcanogenic Nd. Dominance of a different, biogenic source of methane at this site appears unlikely. Analogously to the remaining studied seeps, a thermogenic, intrusion-related origin of methane is suggested here by the moderate ^{13}C-depletion of the seep carbonates, the intimate spatial association between the seep deposit and the underlying volcanic intrusion, including the system of marginal fissures and clastic dykes, and the seep formation in the relatively narrow stratigraphic interval corresponding to the peak of volcanism in the Basque-Cantabrian Basin. Thus, the low degree of the ^{143}Nd-enrichment, together with the marked differences in the δ^{13}C-$\varepsilon_{Nd}(t)$ co-variance patterns observed between the Gorliz and Kardala deposits, point to important differences in the nature of thermal alteration effects associated with the intrusions at these sites.

The principal controls on the influence of igneous intrusions on their host rocks are (i) magmatic heat supply, governed by the primary temperature, cooling rate and size of an intrusion; (ii) depth of the intrusion emplacement; and (iii) host rock properties affecting the type and volume of generated fluids, as well as effectivity of heat transfer: background temperature, content, type and maturation of organic matter, and the presence of potential heat sinks (pore water vaporisation, dehydration/decarbonation reactions; Schutter, 2003; Driesner and Geiger, 2007; Aarnes et al., 2010; Wang et al., 2012; Svensen et al., 2015). When the structural and facies context of the Gorliz deposit is compared with those of the other Basque seeps, a combination of the intrusion size- and depth-related constraints appears particularly likely as key to its geochemical distinctiveness (Fig. 9). In comparison to the estimated volumes of the intrusions underlying the Mutriku-Alkolea and Ispaster deposits, the intrusion at Gorliz is markedly smaller (Table 1). The intrusion size is among the chief controls on the longevity of intrusion-induced hydrothermal circulation and heat transfer (Raymond and Murchison, 1991; Fisher and Narasimhan, 1991; England et al., 1993; Barker et al., 1998; Schofield et al., 2010; Sydnes et al., 2018). For smaller intrusions, the amount of heat transferred to the host rock is typically insufficient to develop a long-lasting hydrothermal system, and only incipient convection develops. This leads to rapid, single-stage volatilisation of pore fluids near the intrusion, followed by rapid cooling of the intrusion-host rock contact by inflow of relatively cool pore waters (Delaney, 1982; Barker et al., 1998). In such cases, the thermal aureoles are typically relatively narrow, limiting both the volume of generated thermogenic methane and interactions between the expelled fluids and the volcanics.

Another factor likely involved in the thermal alteration patterns observed in the studied sections was the intrusion emplacement depth. The intrusion depth dictates several parameters influencing the response of host sediments to contact metamorphism. Arguably most important is the increase in the lithostatic pressure, and associated: (i) decrease in the host rock porosity and permeability, and thus the volume and mobility of pore fluids; and (ii) increase in the boiling point of interstitial water (Delaney, 1982; Polyansky et al., 2003; Schofield et al., 2010; Aarnes et al., 2012). Both these tendencies result in pronounced differences in the cooling styles of very shallow- and moderate-depth intrusions. The conceptual boundary between these two categories is commonly placed at a depth of ~1 km (e.g., Delaney, 1982; Jamtveit et al., 2004; Aarnes et al., 2010; Iyer et al., 2017). Notably, this would translate into differential pathways of contact alteration for the successions underlying the shallowest, Gorliz seep and the remaining deeper, Kardala, Alkolea and Ispaster seeps (Fig. 9). While for the shallowest-level intrusions their thermal influence may result in abrupt expulsion of fluids from the host rock, such hydrothermal systems are typically ephemeral, because vaporisation of the substantial volumes of pore waters available at shallow depths under low-pressure conditions provides a very effective heat sink (Einsele, 1982; Barker et al., 1998; Polyansky et al., 2003; Wang et al., 2012). As a result, thermal influence of very shallow intrusions is commonly very limited (Raymond and Murchison, 1991; England et al., 1993; Driesner and Geiger, 2007). This is in agreement with, on the one hand, the presence at Gorliz of breccia dykes indicative of abrupt overpressure buildup and fluid expulsion (cf., England et al., 1993; Schofield et al., 2010; Aarnes et al., 2012; Cartwright and Santamarina, 2015), and, on the other hand, the limited volume of the seep carbonates produced.

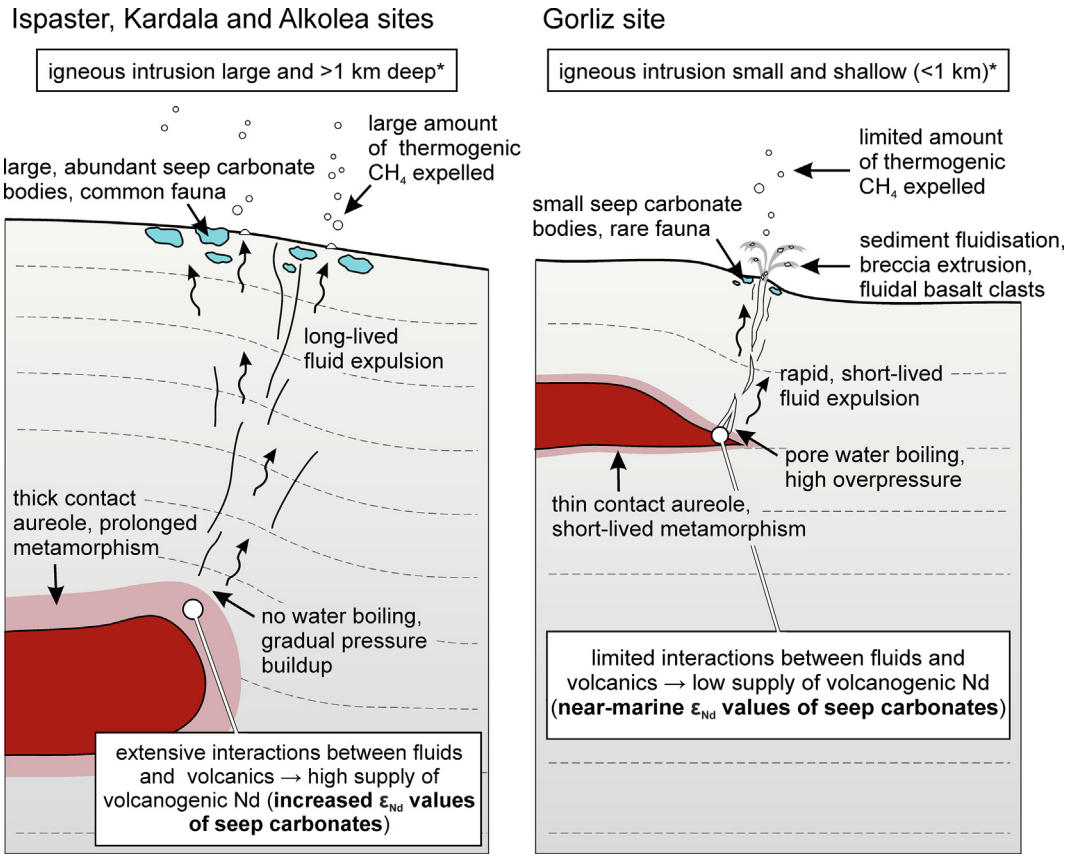

Fig. 9. Proposed relationships among the intrusion characteristics (size, emplacement depth), the nature of resulting fluid expulsion patterns, and the volume, fauna and Nd isotope composition of associated seep carbonates in the Albian Basque-Cantabrian Basin. (*) Note that of additional importance were other constraints, such as the type of intruded sediments (see text for further discussion).

Moreover, the scarcity of chemosynthesis-dependent macrofauna suggests that the system may have been active for too short to support a rich chemosynthesis-based community. The abrupt, early-stage character of the venting is further attested by the extrusion of basalt clasts with fluidal margins, implying their high temperature upon mobilisation (Agirrezabala, 2015). Assuming the temperature-dependence of the $\delta^{18}O_{carbonate}$ signatures, it appears also in line with the low $\delta^{18}O$ values measured in the ^{13}C-enriched cement end-member, suggesting rapid heating and expulsion of the background intersitial fluids. Likewise, rapid dissipation of magmatic heat by water vaporisation is consistent with the relatively thin contact areole (40% of the intrusion thickness) documented around one of the sills underlying the Gorliz deposit (Agirrezabala et al., 2014). Finally, imposed on the effects of the small intrusion size and shallow depth at Gorliz was the effect of the emplacement of the main laccolith within a carbonate-dominated part of the succession, with only subsidiary sills reaching directly into the organic-rich, argillaceous Black Flysch Group (Agirrezabala, 2015; Fig. 4C). Because thermal alteration of limestones by igneous intrusions generally produces limited amounts of, CO_2-, rather than CH_4-dominated, fluids (Aarnes et al., 2011), this further restricted the hydrocarbon-generation potential of this intrusion-host rock system, and possible interactions between the hydrocarbon-rich fluids and the volcanics. These constraints have been recorded in the form of the minor scale of ^{143}Nd-enrichment observed in the Gorliz carbonates.

In contrast, for the Kardala, Alkolea and Ispaster sites, both the larger size of the intrusions, as well as their greater emplacement depths favoured more extensive interactions between the generated fluids and the volcanics (Fig. 9). Emplacement of larger intrusions can be associated with development of convection cells (Delaney, 1982; Fisher and Narasimhan, 1991; Barker et al., 1998). In such cases, continuing recharge of cool interstitial fluids provides a heat-absorbing mechanism aiding in intrusion cooling; a net effect is, however, broader distribution of heat across more extensive contact aureoles (Barker et al., 1998). This favours formation of higher amounts of hydrocarbons, and a more sustained character of their expulsion (cf., Middleton et al., 2001; Schutter, 2003; Sydnes et al., 2018). Furthermore, for intrusions > 1 km deep, the drier nature of the host rock and high temperature required to volatilize pore fluids strongly limits the role of pore water boiling as a heat sink (Raymond and Murchison, 1991; Polyansky et al., 2003; Aarnes et al., 2010; Iyer et al., 2013). Indeed, while for the original depth of the Gorliz intrusion (450 m, i.e., ~45 bar hydrostatic pressure) the boiling point of the interstitial waters could be expected

to fall within the range of 200−250 °C, at the pressures appropriate for the other sites pore water vaporisation would require temperatures at least 100 °C higher. As a result of these depth-related effects, metamorphic aureoles around deeper intrusions are usually thicker, and their thermal influence, with the heat transfer dominated by conduction, rather than water vaporisation, is typically much more persistent (Raymond and Murchison, 1991; Polyansky et al., 2003; Driesner and Geiger, 2007; Aarnes et al., 2015). Accordingly, the intrusions > 1 km deep are the central elements of the models invoking catastrophic thermogenic methane release from sedimented rifts to explain some rapid global climate shifts (Svensen et al., 2004; Aarnes et al., 2010; Iyer et al., 2017). For the Kardala, Alkolea and Ispaster seeps, the more extensive, long-lived character of the contact alteration and associated hydrocarbon discharge is consistent with the high volumes of seep carbonates produced, the presence at Kardala and Ispaster of abundant seep-specialised macrofauna, and the significantly more pronounced presence of volcanogenic, ^{143}Nd-enriched fluid component recorded in their authigenic precipitates.

7. CONCLUSIONS

Neodymium, rare earth element (REE) and stable isotope analyses of four mid-Cretaceous (upper Albian) methane seep deposits formed within an early-stage, sediment-filled rift, the Basque-Cantabrian Basin (northern Spain), have been carried out to provide insight into the relationship between the methane discharge and intrusive igneous activity. In a broader context, the study serves to refine the present understanding of the role of the intrusion characteristics in the nature of associated fluid expulsion, and to assess the general potential of Nd isotopes to record the presence of volcanic-influenced fluids in sedimentary basins subjected to magmatism.

Each of the studied seep deposits is underlain by igneous intrusions, either observed in outcrop (Gorliz deposit), or documented from seismic images (Ispaster, Kardala and Alkolea deposits). Based on indirect evidence, including the distribution of the seep carbonates, their stable isotope composition, and thermal alteration patterns documented for a single sill, it has previously been hypothesised that the seeping methane originated from contact aureoles of the intrusions. Our new approach applying Nd isotope analyses of the seep carbonates provides a direct record of subsurface interactions between the seeping fluids and mafic igneous rocks. For three out of four studied seeps, the $\varepsilon_{Nd}(t)_{carbonate}$ values attest to a former presence of fluids notably enriched in radiogenic, volcanic-derived Nd. The primary character of the carbonate Nd isotope signatures is confirmed by REE analyses, documenting patterns typical of primary seep carbonates. The scale of the ^{143}Nd-enrichment shows high variability both between and within individual sites, apparently reflecting spatial and temporal differences in fluid composition and flow rates, typical of seepage-affected interstitial fluids. The proposed involvement of volcanogenic Nd is in accord with the collected $\delta^{13}C_{carbonate}$ data, suggesting thermogenic origin of the emitted methane, with possible contribution of biogenic methane at the Alkolea site.

The conspicuously less radiogenic $\varepsilon_{Nd}(t)$ values documented for the Gorliz deposit can be most likely attributed to a different style of fluid generation processes controlled by the igneous intrusion at this site. The combination of the relatively small size and shallow emplacement depth of the Gorliz intrusion can be expected to have resulted in rapid heat dissipation by pore water volatilisation, preventing development of sustained hydrothermal circulation. For the larger, deeper intrusions that underlain the Kardala-Alkolea and Ispaster seeps, we propose, in turn, that more extensive thermal alteration of the host sediments, dominated by conduction and convection, enabled development of longer-lived fluid expulsion systems and more extensive interactions between the fluids and volcanics, recorded in the form of increased $\varepsilon_{Nd}(t)_{carbonate}$ values.

The results illustrate the utility of the Nd isotope systematics of seep carbonates to reveal former interactions between seeping fluids and igneous intrusions in sediment-covered rifts. Application of the Nd isotope analyses can, therefore, aid in deconvolving the roles of different triggers in hydrocarbon generation for the very complex fluid circulation systems of the volcanic sedimentary basins.

Declaration of Competing Interest

The authors declare that they have no known competing financial interests or personal relationships that could have appeared to influence the work reported in this paper.

ACKNOWLEDGMENTS

This work was supported by the National Science Centre, Poland (grant No. 2016/23/D/ST10/00444; to MJ), and the Eusko Jaurlaritza (Ikerketa Taldeak IT930-16) and the Spanish State Research Agency (project PID2019-105670GB-I00/AEI/10.13039/501100011033; both to LMA). The authors wish to thank M. Joachimski (Friedrich-Alexander University of Erlangen-Nürnberg) for stable isotope measurements, S. Królikowska-Ciąg ło and A. Walczak (both Adam Mickiewicz University) for assistance during Nd isotope analyses, and S. Kiel (Swedish Museum of Natural History) for discussions. The authors are particularly grateful to two anonymous reviewers and the Associate Editor, B.W. Stewart, for their detailed, helpful suggestions and comments.

APPENDIX A. SUPPLEMENTARY MATERIAL

Supplementary data to this article can be found online at https://doi.org/10.1016/j.gca.2021.03.025.

REFERENCES

Aarnes I., Fristad K., Planke S. and Svensen H. (2011) The impact of host-rock composition on devolatilization of sedimentary rocks during contact metamorphism around mafic sheet intrusions. *Geochem. Geophys. Geosyst.* **12**, 1–11.

Aarnes I., Planke S., Trulsvik M. and Svensen H. (2015) Contact metamorphism and thermogenic gas generation in the Vøring

and Møre basins, offshore Norway, during the Paleocene-Eocene thermal maximum. *J. Geological Soc.* **172**, 588–598.

Aarnes I., Podladchikov Y. and Svensen H. (2012) Devolatilization-induced pressure build-up: Implications for reaction front movement and breccia pipe formation. *Geofluids* **12**, 265–279.

Aarnes I., Svensen H., Connolly J. A. D. and Podladchikov Y. Y. (2010) How contact metamorphism can trigger global climate changes: Modeling gas generation around igneous sills in sedimentary basins. *Geochim. Cosmochim. Acta* **74**, 7179–7195.

Abbott A. N., Haley B. A. and McManus J. (2015) Bottoms up: Sedimentary control of the deep North Pacific Ocean's ε_{Nd} signature. *Geology* **43**, 1035–1038.

Agirrezabala L. M. (2009) Mid-Cretaceous hydrothermal vents and authigenic carbonates in a transform margin, Basque-Cantabrian Basin (western Pyrenees): a multidisciplinary study. *Sedimentology* **56**, 969–996.

Agirrezabala L. M. (2015) Syndepositional forced folding and related fluid plumbing above a magmatic laccolith: Insights from outcrop (Lower Cretaceous, Basque-Cantabrian Basin, western Pyrenees). *Geol. Soc. Am. Bull.* **127**, 982–1000.

Agirrezabala L. M. and Dinarès-Turell J. (2013) Albian syndepositional block rotation and its geological consequences, Basque-Cantabrian Basin (western Pyrenees). *Geol. Mag.* **150**, 986–1001.

Agirrezabala L. M., Dorronsoro C. and Permanyer A. (2008) Geochemical correlation of pyrobitumen fills with host mid-Cretaceous Black Flysch Group (Basque-Cantabrian Basin, western Pyrenees). *Org Geochem.* **39**, 1185–1188.

Agirrezabala L. M. and García-Mondéjar J. (2001) Deep-water fallout tephra deposits in the Black Flysch of Deba (Upper Albian, Basque-Cantabrian Basin). *Geotemas* **3**, 123–126.

Agirrezabala L. M., Kiel S., Blumenberg M., Schäfer N. and Reitner J. (2013) Outcrop analogues of pockmarks and associated methane-seep carbonates: A case study from the Lower Cretaceous (Albian) of the Basque-Cantabrian Basin, western Pyrenees. *Palaeogeogr. Palaeoclimatol. Palaeoecol.* **390**, 94–115.

Agirrezabala L. M., Owen H. G. and García-Mondéjar J. (2002) Syntectonic deposits and punctuated limb rotation in an Albian submarine transpressional fold (Mutriku village, Basque-Cantabrian basin, northern Spain). *GSA Bulletin* **114**, 281–297.

Agirrezabala L. M., Permanyer A., Suárez-Ruiz I. and Dorronsoro C. (2014) Contact metamorphism of organic-rich mudstones and carbon release around a magmatic sill in the Basque-Cantabrian Basin, western Pyrenees. *Org Geochem.* **69**, 26–35.

Agirrezabala L. M., Sarrionandia F. and Carracedo-Sánchez M. (2017) Diatreme-forming volcanism in a deep-water faulted basin margin: Lower Cretaceous outcrops from the Basque-Cantabrian Basin, western Pyrenees. *J. Volcanol. Geoth. Res.* **337**, 124–139.

Angkasa S. S., Jerram D. A., Millett J. M., Svensen H. H., Planke S., Taylor R. A., Schofield N. and Howell J. (2017) Mafic intrusions, hydrothermal venting, and the basalt-sediment transition: Linking onshore and offshore examples from the North Atlantic igneous province. *Interpretation* **5**, SK83-SK101.

Argentino C., Lugli F., Cipriani A., Conti S. and Fontana D. (2019) A deep fluid source of radiogenic Sr and highly dynamic seepage conditions recorded in Miocene seep carbonates of the northern Apennines (Italy). *Chem. Geol.* **522**, 135–147.

Arsouze T., Dutay J. C., Lacan F. and Jeandel C. (2007) Modeling the neodymium isotopic composition with a global ocean circulation model. *Chem. Geol.* **239**, 165–177.

Banner J. L. and Hanson G. N. (1990) Calculation of simultaneous isotopic and trace-element variations during water-rock interactions with applications to carbonate diagenesis. *Geochim. Cosmochim. Acta* **54**, 3123–3137.

Barker C. E., Bone Y. and Lewan M. D. (1998) Fluid inclusion and vitrinite-reflectance geothermometry compared to heat-flow models of maximum paleotemperature next to dikes, western onshore Gippsland Basin, Australia. *Int. J. Coal Geol.* **37**, 73–111.

Bayon G., Birot D., Ruffine L., Caprais J. C., Ponzevera E., Bollinger C., Donval J. P., Charlou J. L., Voisset M. and Grimaud S. (2011) Evidence for intense REE scavenging at cold seeps from the Niger Delta margin. *Earth Planet. Sci. Lett.* **312**, 443–452.

Belka Z., Dopieralska J., Jakubowicz M., Skompski S., Walczak A., Korn D. and Siepak M. (2021) Nd isotope record of ocean closure archived in limestones of the Devonian-Carboniferous carbonate platform, Greater Karatau, southern Kazakhstan. *J. Geol. Soc.* **178**(1), jgs2020-077.

Berndt C., Hensen C., Mortera-Gutierrez C., Sarkar S., Geilert S., Schmidt M., Liebetrau V., Kipfer R., Scholz F., Doll M., Muff S., Karstens J., Planke S., Petersen S., Böttner C., Chi W. C., Moser M., Behrendt R., Fiskal A., Lever M. A., Su C. C., Deng L., Brennwald M. S. and Lizarralde D. (2016) Rifting under steam—How rift magmatism triggers methane venting from sedimentary basins. *Geology* **44**, 767–770.

Birgel D., Feng D., Roberts H. H. and Peckmann J. (2011) Changing redox conditions at cold seeps as revealed by authigenic carbonates from Alaminos Canyon, northern Gulf of Mexico. *Chem. Geol.* **285**, 82–96.

Blaser P., Pöppelmeier F., Schulz H., Gutjahr M., Frank M., Lippold J., Heinrich H., Link J. M., Hoffmann J., Szidat S. and Frank N. (2019) The resilience and sensitivity of Northeast Atlantic deep water εNd to overprinting by detrital fluxes over the past 30,000 years. *Geochim. Cosmochim. Acta* **245**, 79–97.

Campbell K. (2006) Hydrocarbon seep and hydrothermal vent paleoenvironments and paleontology: Past developments and future research directions. *Palaeogeogr. Palaeoclimatol. Palaeoecol.* **232**, 362–407.

Cartwright J. and Santamarina C. (2015) Seismic characteristics of fluid escape pipes in sedimentary basins: Implications for pipe genesis. *Mar. Pet. Geol.* **65**, 126–140.

Castañares L. M., Robles S., Gimeno D. and Vicente-Bravo J. C. (2001) The submarine volcanic system of the Errigoiti Formation (Albian–Santonian of the Basque-Cantabrian Basin, northern Spain): stratigraphic framework, facies and sequences. *J. Sediment. Res.* **71**, 318–333.

Chavagnac V., Saleban Ali H., Jeandel C., Leleu T., Destrigneville C., Castillo A., Cotte L., Waeles M., Cathalot C., Laes-Huon A., Pelleter E., Nonnotte P., Sarradin P.-M. and Cannat M. (2018) Sulfate minerals control dissolved rare earth element flux and Nd isotope signature of buoyant hydrothermal plume (EMSO-Azores, 37°N Mid-Atlantic Ridge). *Chem. Geol.* **499**, 111–125.

Craddock P. R., Bach W., Seewald J. S., Rouxel O. J., Reeves E. and Tivey M. K. (2010) Rare earth element abundances in hydrothermal fluids from the Manus Basin, Papua New Guinea: Indicators of sub-seafloor hydrothermal processes in back-arc basins. *Geochim. Cosmochim. Acta* **74**, 5494–5513.

Cruse A. M. and Seewald J. S. (2006) Geochemistry of low-molecular weight hydrocarbons in hydrothermal fluids from Middle Valley, northern Juan de Fuca Ridge. *Geochim. Cosmochim. Acta* **70**, 2073–2092.

Dählmann A. and de Lange G. J. (2003) Fluid–sediment interactions at Eastern Mediterranean mud volcanoes: a stable isotope study from ODP Leg 160. *Earth Planet. Sci. Lett.* **212**, 377–391.

DeFelipe I., Pedreira D., Pulgar J. A., Iriarte E. and Mendia M. (2017) Mantle exhumation and metamorphism in the Basque-Cantabrian Basin (NSpain): Stable and clumped isotope analysis in carbonates and comparison with ophicalcites in

the North-Pyrenean Zone (Urdach and Lherz). *Geochem. Geophys. Geosyst.* **18**, 631–652.

DeFelipe I., Pulgar J. A. and Pedreira D. (2018) Crustal structure of the eastern Basque-Cantabrian Zone - western Pyrenees: from the Cretaceous hyperextension to the Cenozoic inversion. *Revisita de la Sociedad Geológica de España* **31**, 69–82.

Delaney P. T. (1982) Rapid intrusion of magma into wet rock: Groundwater flow due to pore pressure increases. *J. Geophys. Res.* **87**, 7739.

Douville E., Bienvenu P., Charlou J. L., Donval J. P., Fouquet Y., Appriou P. and Gamo T. (1999) Yttrium and rare earth elements in fluids from various deep-sea hydrothermal systems. *Geochim. Cosmochim. Acta* **63**, 627–643.

Driesner T. and Geiger S. (2007) Numerical simulation of multiphase fluid flow in hydrothermal systems. *Rev. Mineral. Geochem.* **65**, 187–212.

Du J., Haley B. A. and Mix A. C. (2016) Neodymium isotopes in authigenic phases, bottom waters and detrital sediments in the Gulf of Alaska and their implications for paleo-circulation reconstruction. *Geochim. Cosmochim. Acta* **193**, 14–35.

Dulski P. (1994) Interferences of oxide, hydroxide and chloride analyte species in the determination of rare earth elements in geological samples by inductively coupled plasma-mass spectrometry. *J. Anal. Chem.* **350**, 194–203.

EEE (2003) *1:25000 Eskalako Euskal Herriko Mapa Geologikoa*. Eusko Jaurlaritza, Bilbo.

Einsele G. (1982) Mechanism of sill intrusion into soft sediment and expulsion of pore water. *Deep Sea Drilling Project, Initial Reports* **64**, 1169–1176.

Einsele G. (2000) *Sedimentary Basins: Evolution, Facies, and Sediment Budget*. Springer, Berlin Heidelberg.

Einsele G., Gieskes J. M., Curray J., Moore D. M., Aguayo E., Aubry M.-P., Fornari D., Guerrero J., Kastner M., Kelts M., Lyle M., Matoba Y., Molina-Cruz A., Niemitz J., Rueda J., Saunders A., Schrader H., Simoneit B. R. T. and Vacquier V. (1980) Intrusion of basaltic sills into highly porous sediments, and resulting hydrothermal activity. *Nature* **283**, 441–445.

England R. W., Butler R. W. H. and Hutton D. H. W. (1993) The role of Paleocene magmatism in the Tertiary evolution of basins on the NW seaboard. In *Petroleum Geology of Northwest Europe: Proceedings of the 4th Conference. The Geological Society* (ed. J. R. Parker), pp. 97–105.

Fanton K. C., Holmden C., Nowlan G. S. and Haidl F. M. (2002) $^{143}Nd/^{144}Nd$ and Sm/Nd stratigraphy of Upper Ordovician epeiric sea carbonates. *Geochim. Cosmochim. Acta* **66**, 241–255.

Fisher A. T. and Narasimhan T. N. (1991) Numerical simulations of hydrothermal circulation resulting from basalt intrusions in a buried spreading center. *Earth Planet. Sci. Lett.* **103**, 100–115.

Freslon N., Bayon G., Toucanne S., Bermell S., Bollinger C., Chéron S., Etoubleau J., Germain Y., Khripounoff A., Ponzevera E. and Rouget M.-L. (2014) Rare earth elements and neodymium isotopes in sedimentary organic matter. *Geochim. Cosmochim. Acta* **140**, 177–198.

Friedman I. and O'Neil J. R. (1977) Compilation of stable isotope fractionation factors of geochemical interest. *U.S. Geol. Surv. Prof. Pap.* **440-K**, 1–12.

Fröllje H., Pahnke K., Schnetger B., Brumsack H.-J., Dulai H. and Fitzsimmons J. N. (2016) Hawaiian imprint on dissolved Nd and Ra isotopes and rare earth elements in the central North Pacific: Local survey and seasonal variability. *Geochim. Cosmochim. Acta* **189**, 110–131.

Gaillard C., Rio M., Rolin Y. and Roux M. (1992) Fossil chemosynthetic communities related to vents or seeps in sedimentary basins: the pseudobioherms of southeastern France compared to other world examples. *Palaios* **7**, 451–465.

García-Mondéjar J. (1990) The Aptian-Albian carbonate episode of the Basque-Cantabrian Basin (northern Spain): general characteristics, controls and evolution. In *Carbonate Platforms: Facies* (eds. M. E. Tucker, J. L. Wilson, P. D. Crevello, J. R. Sarg and J. F. Read). Special Publications of the International Association of Sedimentologists, Sequences and Evolution, pp. 257–290.

García-Mondéjar J., Agirrezabala L. M., Aranburu A., Fernández-Mendiola P. A., Gómez-Pérez I., López-Horgue M. A. and Rosales I. (1996) Aptian-Albian Tectonic pattern of the Basque-Cantabrian Basin (northern Spain). *Geol. J.* **31**, 13–45.

García-Mondéjar, J., Fernandez-Mendiola, P.A., Agirrezabala, L. M., Aranburu, A., López-Horgue, M.A., Iriarte, E., Martínez de Rituerto, S. (2004) El Aptiense-Albiense de la Cuenca Vasco-Cantábrica, in: Vera, J.A. (Ed.), Geología de España, pp. 291-296.

García-Mondéjar J. and Robador A. (1986–87) Sedimentación y paleogeografía del Complejo Urgoniano (Aptiense-Albiense) en el área de Bermeo (region Vasco-Cantábrica septentrional). *Acta Geológica Hispánica* **21–22**, 411–441.

García-Mondéjar J., Carracedo-Sánchez M., Owen H. G., Fernández-Mendiola P. A. and Somerville I. D. (2018) The Early Aptian volcanic episode of Gutiolo (N Spain): Expression of the Bilbao Rift Fault Zone. *Geol. J.* **54**, 3509–3526.

Ge L., Chen W., Zhu B., Fan M., Yang T. and Jiang S. (2020) Sr and Nd isotopes of cold seep carbonates from the northern South China sea as proxies for fluid sources. *Mar. Pet. Geol.* **115** 104284.

Geilert S., Hensen C., Schmidt M., Liebetrau V., Scholz F., Doll M., Deng L., Fiskal A., Lever M. A., Su C.-C., Schloemer S., Sarkar S., Thiel V. and Berndt C. (2018) On the formation of hydrothermal vents and cold seeps in the Guaymas Basin, Gulf of California. *Biogeosciences* **15**, 5715–5731.

Goldstein S. L. and Jacobsen S. B. (1988) Nd and Sr isotopic systematics of river water suspended material: implications for crustal evolution. *Earth Planet. Sci. Lett.* **87**, 249–265.

Gutjahr M., Frank M., Stirling C. H., Klemm V., van de Flierdt T. and Halliday A. N. (2007) Reliable extraction of a deepwater trace metal isotope signal from Fe–Mn oxyhydroxide coatings of marine sediments. *Chem. Geol.* **242**, 351–370.

Haley B. A., Klinkhammer G. P. and McManus J. (2004) Rare earth elements in pore waters of marine sediments. *Geochim. Cosmochim. Acta* **68**, 1265–1279.

Hensen C., Wallmann K., Schmidt M., Ranero C. R. and Suess E. (2004) Fluid expulsion related to mud extrusion off Costa Rica—A window to the subducting slab. *Geology* **32**, 201–204.

Himmler T., Bach W., Bohrmann G. and Peckmann J. (2010) Rare earth elements in authigenic methane-seep carbonates as tracers for fluid composition during early diagenesis. *Chem. Geol.* **277**, 126–136.

Holmden C., Mitchell C. E., LaPorte D. F., Patterson W. P., Melchin M. J. and Finney S. C. (2013) Nd isotope records of late Ordovician sea-level change—Implications for glaciation frequency and global stratigraphic correlation. *Palaeogeogr. Palaeoclimatol. Palaeoecol.* **386**, 131–144.

Horikawa K., Martin E. E., Asahara Y. and Sagawa T. (2011) Limits on conservative behavior of Nd isotopes in seawater assessed from analysis of fish teeth from Pacific core tops. *Earth Planet. Sci. Lett.* **310**, 119–130.

Huedo-Cuesta J. L., Cole C., Pérez-García A., Zucconi V., Clauss O., Sese-Martínez V. H. and Muskaj J. S. (2009) Construcción del modelo de velocidades para el procesado en profundidad de la sísmica de la Fragata 3D (plataforma y talud continentales de Vizcaya). In *6th Simposio Margen Ibérico Atlántico*, pp. 93–96.

Iyer K., Rüpke L. and Galerne C. Y. (2013) Modeling fluid flow in sedimentary basins with sill intrusions: Implications for

hydrothermal venting and climate change. *Geochem. Geophys. Geosyst.* **14**, 5244–5262.

Iyer K., Schmid D. W., Planke S. and Millett J. (2017) Modelling hydrothermal venting in volcanic sedimentary basins: Impact on hydrocarbon maturation and paleoclimate. *Earth Planet. Sci. Lett.* **467**, 30–42.

Jacobsen S. B. and Wasserburg G. J. (1980) Sm-Nd isotopic evolution of chondrites. *Earth Planet. Sci. Lett.* **50**, 139–155.

Jaffrés J. B. D., Shields G. A. and Wallmann K. (2007) The oxygen isotope evolution of seawater: A critical review of a long-standing controversy and an improved geological water cycle model for the past 3.4 billion years. *Earth Sci. Rev.* **83**, 83–122.

Jakubowicz M., Dopieralska J. and Belka Z. (2015) Tracing the composition and origin of fluids at an ancient hydrocarbon seep (Hollard Mound, Middle Devonian, Morocco): A Nd, REE and stable isotope study. *Geochim. Cosmochim. Acta* **156**, 50–74.

Jakubowicz M., Hryniewicz K. and Belka Z. (2017) Mass occurrence of seep-specific bivalves in the oldest-known cold seep metazoan community. *Sci. Rep.* **7**, 14292.

Jakubowicz M., Dopieralska J., Kaim A., Skupien P., Kiel S. and Belka Z. (2019) Nd isotope composition of seep carbonates: Towards a new approach for constraining subseafloor fluid circulation at hydrocarbon seeps. *Chem. Geol.* **503**, 40–51.

Jakubowicz M., Kiel S., Goedert J. L., Dopieralska J. and Belka Z. (2020) Fluid expulsion system and tectonic architecture of the incipient Cascadia convergent margin as revealed by Nd, Sr and stable isotope composition of mid-Eocene methane seep carbonates. *Chem. Geol.* **558** 119872.

Jammes S., Manatschal G., Lavier L. and Masini E. (2009) Tectonosedimentary evolution related to extreme crustal thinning ahead of a propagating ocean: Example of the western Pyrenees. *Tectonics* **28**, TC4012.

Jamtveit B., Svensen H., Podladchikov Y. and Planke S. (2004) Hydrothermal vent complexes associated with sill intrusions in sedimentary basins. In *Physical Geology of High-Level Magmatic Systems* (eds. C. Breitkreuz and N. Petford). Geological Society, London, Special Publications, pp. 233–241.

Jarvis I. A. N., Gale A. S., Jenkyns H. C. and Pearce M. A. (2006) Secular variation in Late Cretaceous carbon isotopes: a new $\delta^{13}C$ carbonate reference curve for the Cenomanian-Campanian (99.6–70.6 Ma). *Geol. Mag.* **143**, 561–608.

Jenkins R. G., Kaim A., Hikida Y. and Kiel S. (2018) Four new species of the Jurassic to Cretaceous seep-restricted bivalve *Caspiconcha* and implications for the history of chemosynthetic communities. *J. Paleontol.* **92**, 596–610.

Kawagucci S., Ueno Y., Takai K., Toki T., Ito M., Inoue K., Makabe A., Yoshida N., Muramatsu Y., Takahata N., Sano Y., Narita T., Teranishi G., Obata H., Nakagawa S., Nunoura T. and Gamo T. (2013) Geochemical origin of hydrothermal fluid methane in sediment-associated fields and its relevance to the geographical distribution of whole hydrothermal circulation. *Chem. Geol.* **339**, 213–225.

Kiel S. (2013) Lucinid bivalves from ancient methane seeps. *J. Molluscan Stud.* **79**, 346–363.

Kim J.-H., Torres M. E., Haley B. A., Kastner M., Pohlman J. W., Riedel M. and Lee Y.-J. (2012) The effect of diagenesis and fluid migration on rare earth element distribution in pore fluids of the northern Cascadia accretionary margin. *Chem. Geol.* **291**, 152–165.

Knauth L. P. and Kennedy M. J. (2009) The late Precambrian greening of the Earth. *Nature* **460**, 728–732.

Knittel K. and Boetius A. (2009) Anaerobic oxidation of methane: progress with an unknown process. *Annu. Rev. Microbiol.* **63**, 311–334.

Lacan F. and Jeandel C. (2005) Neodymium isotopes as a new tool for quantifying exchange fluxes at the continent–ocean interface. *Earth Planet. Sci. Lett.* **232**, 245–257.

Lawrence J. R., Drever J. I., Anderson T. F. and Brueckner H. K. (1979) Importance of alteration of volcanic material in the sediments of Deep Sea Drilling Site 323: chemistry, $^{18}O/^{16}O$ and $^{87}Sr/^{86}Sr$. *Geochim. Cosmochim. Acta* **43**, 573–588.

Lawrence J. R. and Gieskes J. M. (1981) Constraints on water transport and alteration in the oceanic crust from the isotopic composition of pore water. *J. Geophys. Res. Solid Earth* **86**, 7924–7934.

Lawrence M. G., Greig A., Collerson K. D. and Kamber B. S. (2006) Rare earth element and yttrium variability in South East Queensland waterways. *Aquat. Geochem.* **12**, 39–72.

Liu X.-M., Hardisty D. S., Lyons T. W. and Swart P. K. (2019) Evaluating the fidelity of the cerium paleoredox tracer during variable carbonate diagenesis on the Great Bahamas Bank. *Geochim. Cosmochim. Acta* **248**, 25–42.

Lizarralde D., Soule S. A., Seewald J. and Proskurowski G. (2011) Carbon release by off-axis magmatism in a young sedimented spreading centre. *Nat. Geosci.* **4**, 50–54.

López-Horgue M. A., Iriarte E., Schröder S., Fernández-Mendiola P. A., Caline B., Corneyllie H., Frémont J., Sudrie M. and Zerti S. (2010) Structurally controlled hydrothermal dolomites in Albian carbonates of the Asón valley, Basque Cantabrian Basin, Northern Spain. *Mar. Pet. Geol.* **27**, 1069–1092.

Machel H. G. (2004) Concepts and models of dolomitization: a critical reappraisal. In *The Geometry and Petrogenesis of Dolomite Hydrocarbon Reservoirs* (eds. C. J. R. Braithwaite, G. Rizzi and G. Darke). Geological Society, London, Special Publications, pp. 7–63.

Marshall J. D. (1992) Climatic and oceanographic isotopic signals from the carbonate rock record and their preservation. *Geol. Mag.* **129**, 143–160.

Martin E. E., Blair S. W., Kamenov G. D., Scher H. D., Bourbon E., Basak C. and Newkirk D. N. (2010) Extraction of Nd isotopes from bulk deep sea sediments for paleoceanographic studies on Cenozoic time scales. *Chem. Geol.* **269**, 414–431.

McLennan S. M. (1989) Rare-earth elements in sedimentary rocks - influence of provenance and sedimentary processes. *Rev. Mineral.* **21**, 169–200.

Middleton D. W. J., Parnell J., Green P. F., Xu G. and McSherry M. (2001) Hot fluid flow events in Atlantic margin basins: an example from the Rathlin Basin. In *The Petroleum Exploration of Ireland's Offshore Basins* (eds. E. M. Haughton and D. V. Corcoran). The Geological Society, London, Special Publications, pp. 91–105.

Molina-Kescher M., Frank M. and Hathorne E. C. (2014) Nd and Sr isotope compositions of different phases of surface sediments in the South Pacific: Extraction of seawater signatures, boundary exchange, and detrital/dust provenance. *Geochem. Geophys. Geosyst.* **15**, 3502–3520.

Naehr T. H., Eichhubl P., Orphan V. J., Hovland M., Paull C. K., Ussler W., Lorenson T. D. and Greene H. G. (2007) Authigenic carbonate formation at hydrocarbon seeps in continental margin sediments: A comparative study. *Deep Sea Res. Part II* **54**, 1268–1291.

Núñez-Useche F., Canet C., Liebetrau V., Puig T. P., Ponciano A. C., Alfonso P., Berndt C., Hensen C., Mortera-Gutierrez C. and Rodríguez-Díaz A. A. (2018) Redox conditions and authigenic mineralization related to cold seeps in central Guaymas Basin, Gulf of California. *Mar. Pet. Geol.* **95**, 1–15.

Orphan V. J., Ussler W., Naehr T. H., House C. H., Hinrichs K. U. and Paull C. K. (2004) Geological, geochemical, and microbiological heterogeneity of the seafloor around methane vents in

the Eel River Basin, offshore California. *Chem. Geol.* **205**, 265–289.

Paull C. K., Ussler W., Peltzer E. T., Brewer P. G., Keaten R., Mitts P. J., Nealon J. W., Greinert J., Herguera J.-C. and Elena Perez M. (2007) Authigenic carbon entombed in methane-soaked sediments from the northeastern transform margin of the Guaymas Basin, Gulf of California. *Deep Sea Res. Part II* **54**, 1240–1267.

Peckmann J. and Thiel V. (2004) Carbon cycling at ancient methane–seeps. *Chem. Geol.* **205**, 443–467.

Peckmann J., Birgel D. and Kiel S. (2009) Molecular fossils reveal fluid composition and flow intensity at a Cretaceous seep. *Geology* **37**, 847–850.

Pedrera A., García-Senz J., Ayala C., Ruiz-Constán A., Rodríguez-Fernández L. R., Robador A. and González Menéndez L. (2017) Reconstruction of the Exhumed Mantle Across the North Iberian Margin by Crustal-Scale 3-D Gravity Inversion and Geological Cross Section. *Tectonics* **36**, 3155–3177.

Piepgras D. J. and Wasserburg G. J. (1980) Neodymium isotopic variations in seawater. *Earth Planet. Sci. Lett.* **50**, 128–138.

Piepgras D. J. and Wasserburg G. J. (1985) Strontium and neodymium isotopes in hot springs on the East Pacific Rise and Guaymas Basin. *Earth Planet. Sci. Lett.* **72**, 341–356.

Planke S., Rasmussen T., Rey S. S. and Myklebust R. (2005) Seismic characteristics and distribution of volcanic intrusions and hydrothermal vent complexes in the Vøring and Møre basins. In *Petroleum Geology: North-West Europe and Global Perspectives - Proceedings of the 6th Petroleum Geology Conference* (eds. A. Doré and B. Vining). Geological Society, London, pp. 833–844.

Polyansky O. P., Reverdatto V. V., Khomenko A. V. and Kuznetsova E. N. (2003) Modeling of fluid flow and heat transfer induced by basaltic near-surface magmatism in the Lena-Tunguska petroleum basin (Eastern Siberia, Russia). *J. Geochem. Explor.* **78–79**, 687–692.

Rat P. (1988) The Basque-Cantabrian basin between the Iberian and European plates. Some fact but still many problems. *Revista de la Sociedad Geológica de España* **1**, 327–348.

Raymond A. C. and Murchison D. G. (1991) The relationship between organic maturation, the widths of thermal aureoles and the thicknesses of sills in the Midland Valley of Scotland and Northern England. *J. Geol. Soc.* **148**, 215–218.

Rodriguez Lazaro J., Pascual A. and Elorza J. (1998) Cenomanian events in the deep western Basque Basin: the Leioa section. *Cretac. Res.* **19**, 673–700.

Rongemaille E., Bayon G., Pierre C., Bollinger C., Chu N. C., Fouquet Y., Riboulot V. and Voisset M. (2011) Rare earth elements in cold seep carbonates from the Niger delta. *Chem. Geol.* **286**, 196–206.

Rossy M., Azambre B. and Albarede F. (1992) REE and Sr-Nd isotope geochemistry of the alkaline magmatism from the Cretaceous North Pyrenean Rift Zone (France-Spain). *Chem. Geol.* **97**, 33–46.

Schofield N., Holford S., Millett J., Brown D., Jolley D., Passey S. R., Muirhead D., Grove C., Magee C., Murray J., Hole M., Jackson C. A. L. and Stevenson C. (2017) Regional magma plumbing and emplacement mechanisms of the Faroe-Shetland Sill Complex: implications for magma transport and petroleum systems within sedimentary basins. *Basin Res.* **29**, 41–63.

Schofield N., Stevenson C. and Reston T. (2010) Magma fingers and host rock fluidization in the emplacement of sills. *Geology* **38**, 63–66.

Schutter S. R. (2003) Hydrocarbon occurrence and exploration in and around igneous rocks. In *Hydrocarbons in Crystalline Rocks* (eds. N. Petford and K. J. W. McCaffrey). Geological Society, London, Special Publications, pp. 7–33.

Seewald J. S., Seyfried W. E. and Shanks, III, W. C. (1994) Variations in the chemical and stable isotope composition of carbon and sulfur species during organic-rich sediment alteration: An experimental and theoretical study of hydrothermal activity at Guaymas Basin, Gulf of California. *Geochim. Cosmochim. Acta* **58**, 5065–5082.

Shaw H. F. and Wasserburg G. J. (1985) Sm-Nd in marine carbonates and phosphates - implications for Nd isotopes in seawater and crustal ages. *Geochim. Cosmochim. Acta* **49**, 503–518.

Simoneit B. R. T. (1994) Organic matter alteration and fluid migration in hydrothermal systems. In *Geofluids: Origin* (ed. J. Parnell). Geological Society Special Publications, Migration and Evolution of Fluids in Sedimentary Basins, pp. 261–274.

Simoneit B. R. T., Kawka O. E. and Brault M. (1988) Origin of gases and condensates in the Guaymas Basin hydrothermal system (Gulf of California). *Chem. Geol.* **71**, 169–182.

Snyder G. T., Sano Y., Takahata N., Matsumoto R., Kakizaki Y. and Tomaru H. (2020) Magmatic fluids play a role in the development of active gas chimneys and massive gas hydrates in the Japan Sea. *Chem. Geol.* **535** 119462.

Souquet P., Debroas E. J., Boirie J. M., Pons P., Fixari G., Roux J. C., Dol J., Thieuloy J. P., Bonnemaison M., Manivit H. and Peybernes B. (1985) Le Groupe du Flysch Noir (Albo-Cenomanien) dans les Pyrenees. *Bulletin du Centre de recherches Elf Exploration Production* **9**, 183–252.

Soyol-Erdene T.-O. and Huh Y. (2013) Rare earth element cycling in the pore waters of the Bering Sea Slope (IODP Exp. 323). *Chem. Geol.* **358**, 75–89.

Stichel T., Pahnke K., Duggan B., Goldstein S. L., Hartman A. E., Paffrath R. and Scher H. D. (2018) TAG plume: revisiting the hydrothermal neodymium contribution to seawater. *Front. Mar. Sci.* **5**, 96.

Stolper D. A., Lawson M., Davis C. L., Ferreira A. A., Santos Neto E. V., Ellis G. S., Lewan M. D., Martini A. M., Tang Y., Schoell M., Sessions A. L. and Eiler J. M. (2014) Formation temperatures of thermogenic and biogenic methane. *Science* **344**, 1500–1503.

Sturz A. A., Sturdivant A. E., Leif R. N., Simoneit B. R. T. and Gieskes J. M. (1996) Evidence for retrograde hydrothermal reactions in near surface sediments of Guaymas Basin, Gulf of California. *Appl. Geochem.* **11**, 645–665.

Svensen H., Fristad K. E., Polozov A. G. and Planke S. (2015) Volatile generation and release from continental large igneous provinces. In *Volcanism and Global Environmental Change* (eds. A. Schmidt, K. Fristad and L. T. Elkins-Tanton). Cambridge University Press, pp. 177–192.

Svensen H., Planke S., Chevallier L., Malthe-Sørenssen A., Corfu F. and Jamtveit B. (2007) Hydrothermal venting of greenhouse gases triggering Early Jurassic global warming. *Earth Planet. Sci. Lett.* **256**, 554–566.

Svensen H., Planke S., Malthe-Sørenssen A., Jamtveit B., Myklebust R., Rasmussen Eidem T. and Rey S. S. (2004) Release of methane from a volcanic basin as a mechanism for initial Eocene global warming. *Nature* **429**, 542–545.

Sydnes M., Fjeldskaar W., Løtveit I. F., Grunnaleite I. and Cardozo N. (2018) The importance of sill thickness and timing of sill emplacement on hydrocarbon maturation. *Mar. Pet. Geol.* **89**, 500–514.

Tachikawa K., Arsouze T., Bayon G., Bory A., Colin C., Dutay J.-C., Frank N., Giraud X., Gourlan A. T., Jeandel C., Lacan F., Meynadier L., Montagna P., Piotrowski A. M., Plancherel Y., Pucéat E., Roy-Barman M. and Waelbroeck C. (2017) The large-scale evolution of neodymium isotopic composition in the global modern and Holocene ocean revealed from seawater and archive data. *Chem. Geol.* **457**, 131–148.

Teixell A., Labaume P., Ayarza P., Espurt N., de Saint Blanquat M. and Lagabrielle Y. (2018) Crustal structure and evolution of the Pyrenean-Cantabrian belt: A review and new interpretations from recent concepts and data. *Tectonophysics* **724–725**, 146–170.

Teske A., McKay L. J., Ravelo A. C., Aiello I., Mortera C., Nunez-Useche F., Canet C., Chanton J. P., Brunner B., Hensen C., Ramirez G. A., Sibert R. J., Turner T., White D., Chambers C. R., Buckley A., Joye S. B., Soule S. A. and Lizarralde D. (2019) Characteristics and Evolution of sill-driven off-axis hydrothermalism in Guaymas Basin - the Ringvent site. *Sci. Rep.* **9**, 13847.

Tibaldi A., Pasquarè F. and Tormey D. (2010) Volcanism in reverse and strike-slip fault settings. In *New Frontiers in Integrated Solid Earth Science* (eds. S. Cloethingh and J. Negendank). Springer-Verlag, pp. 315–348.

Tissot B. P. and Welte D. H. (1978) *Petroleum Formation and Occurrence*. Springer-Verlag.

Tugend J., Manatschal G., Kusznir N. J. and Masini E. (2015) Characterizing and identifying structural domains at rifted continental margins: application to the Bay of Biscay margins and its Western Pyrenean fossil remnants. *Geological Society, London, Special Publications* **413**, 171–203.

Ubide T. *The Cretaceous alkaline magmatism in northeast Iberia: igneus processes and geodynamic implications*. PhD Thesis, Universidad de Zaragoza, Facultad de Ciencias.

Ubide T., Wijbrans J. R., Galé C., Arranz E., Lago M. and Larrea P. (2014) Age of the Cretaceous alkaline magmatism in northeast Iberia: Implications for the Alpine cycle in the Pyrenees. *Tectonics* **33**, 1444–1460.

Velasco F., Herrero J. M., Yusta I., Alonso J. A., Seebold I. and Leach D. (2003) Geology and geochemistry of the Reocín zinc-lead deposit, Basque Cantabrian Basin, northern Spain. *Econ. Geol.* **98**, 1371–1396.

Wang D., Song Y., Liu Y., Zhao M., Qi T. and Liu W. (2012) The influence of igneous intrusions on the peak temperatures of host rocks: Finite-time emplacement, evaporation, dehydration, and decarbonation. *Comput. Geosci.* **38**, 99–106.

Webb G. E., Nothdurft L. D., Kamber B. S., Kloprogge J. T. and Zhao J.-X. (2009) Rare earth element geochemistry of scleractinian coral skeleton during meteoric diagenesis: a sequence through neomorphism of aragonite to calcite. *Sedimentology* **56**, 1433–1463.

Welhan J. A. and Lupton J. E. (1987) Light Hydrocarbon Gases in Guaymas Basin Hydrothermal Fluids: Thermogenic Versus Abiogenic Origin. *AAPG Bull.* **71**, 215–223.

Whiticar M. J. (1999) Carbon and hydrogen isotope systematics of bacterial formation and oxidation of methane. *Chem. Geol.* **161**, 291–314.

Wiese F., Kiel S., Pack A., Walliser E. O. and Agirrezabala L. M. (2015) The beast burrowed, the fluid followed – Crustacean burrows as methane conduits. *Mar. Pet. Geol.* **66**, 631–640.

Zwicker J., Smrzka D., Himmler T., Monien P., Gier S., Goedert J. L. and Peckmann J. (2018) Rare earth elements as tracers for microbial activity and early diagenesis: A new perspective from carbonate cements of ancient methane-seep deposits. *Chem. Geol.* **501**, 77–85.

Associate editor: Brian W. Stewart